



### 저작자표시 2.0 대한민국

이용자는 아래의 조건을 따르는 경우에 한하여 자유롭게

- 이 저작물을 복제, 배포, 전송, 전시, 공연 및 방송할 수 있습니다.
- 이차적 저작물을 작성할 수 있습니다.
- 이 저작물을 영리 목적으로 이용할 수 있습니다.

다음과 같은 조건을 따라야 합니다:



저작자표시. 귀하는 원저작자를 표시하여야 합니다.

- 귀하는, 이 저작물의 재이용이나 배포의 경우, 이 저작물에 적용된 이용허락조건을 명확하게 나타내어야 합니다.
- 저작권자로부터 별도의 허가를 받으면 이러한 조건들은 적용되지 않습니다.

저작권법에 따른 이용자의 권리는 위의 내용에 의하여 영향을 받지 않습니다.

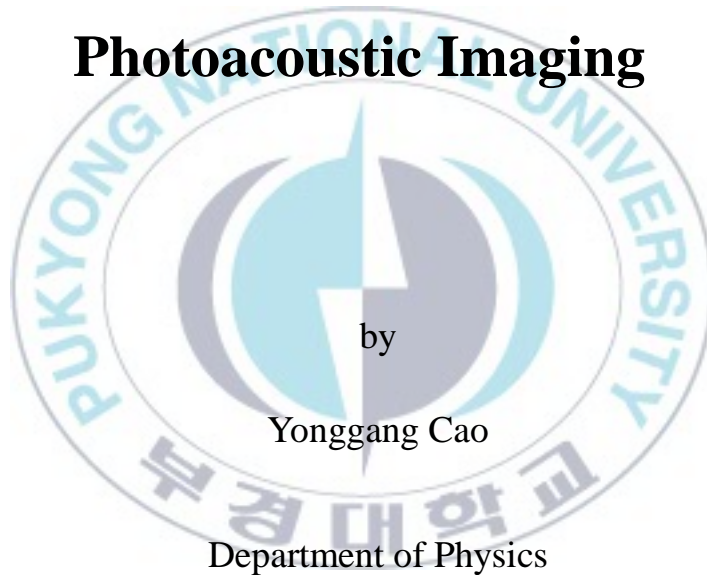
이것은 [이용허락규약\(Legal Code\)](#)을 이해하기 쉽게 요약한 것입니다.

[Disclaimer](#)

Thesis for the Degree of

Doctor of Philosophy

**Ultrasound Transducers by Using  
PVDF and PMN-PZT for  
Photoacoustic Imaging**



Yonggang Cao

Department of Physics

The Graduate School

Pukyong National University

February 2015

# Ultrasound Transducers by Using PVDF and PMN-PZT for Photoacoustic Imaging

(광음향 영상화를 위한 PVDF와  
PMN-PZT 초음파 트랜스듀서 개발)

Advisor: Prof. Kang Lyeol Ha

by

Yonggang Cao

A thesis submitted in partial fulfillment of the requirements for the  
degree of

Doctor of Philosophy

in Department of Physics, The Graduate School,  
Pukyong National University

February 2015

**Ultrasound Transducers by Using PVDF and PMN-PZT  
for Photoacoustic Imaging**

A dissertation

by

Yonggang Cao

Approved by:

Moo-Joon Kim

(Chairman)

Jong-Rak Yoon

(Member)

Hyunwook Kang

(Member)

Jung-soon Kim

(Member)

Kang-Lyeol Ha

(Member)



February 27, 2015

# Contents

List of Figures.....	iv
List of Tables.....	vi
Abstract.....	vii
1. Introduction .....	1
1.1. Background .....	1
1.2. Aims and Outline.....	3
2. Photoacoustic Imaging .....	5
2.1. PA effect .....	5
2.2. PA imaging system .....	8
2.2.1. Optical excitation.....	8
2.2.2. Acoustic detection .....	10
2.2.3. Reconstruction .....	12
2.2.4. Development of PA imaging system.....	12
2.3. Classification of PA imaging .....	16
2.3.1. 2-D PA imaging .....	16
2.3.2. 3-D PA imaging .....	18
2.3.3. Real-time PA imaging.....	20
2.4. Influence factors on PA imaging.....	21
2.5. Summary .....	22
3. Piezoelectric transducers for PA imaging .....	23
3.1. Piezoelectric transducers and PA imaging applications.....	23
3.1.1. Polymer transducer .....	23
3.1.2. Single crystal transducer.....	25
3.1.3. Ceramic transducer .....	27
3.2. Transducer fabrication for PA imaging.....	29
3.2.1. Single element transducers .....	30

3.2.1.1. PVDF transducer .....	30
3.2.1.2. PMN-PZT transducer.....	32
3.2.2. Circular array transducers.....	34
3.2.2.1. PVDF transducer .....	34
3.2.2.2. PMN-PZT transducer.....	37
3.3. Summary .....	38
4. Characteristics of the fabricated transducers .....	39
4.1. Pulse-echo response.....	39
4.1.1. Single element transducers .....	39
4.1.1.1. Experiments.....	39
4.1.1.2. Results .....	41
4.1.2. Circular array transducers.....	42
4.1.2.1. Experiments.....	42
4.1.2.2. Results .....	44
4.2. Receiving sensitivity .....	46
4.2.1. Single element transducers .....	46
4.2.1.1. Experiments.....	46
4.2.1.2. Results .....	47
4.2.2. Circular array transducers.....	49
4.2.2.1. Experiments.....	49
4.2.2.2. Results .....	50
4.3. Summary .....	52
5. PA imaging .....	53
5.1. Scanning acoustic microscopy approach.....	53
5.1.1. Imaging system.....	53
5.1.2. Experiment.....	55
5.1.3. Results .....	56
5.1.3.1. Single element transducers .....	56

5.1.3.2. Circular array transducers.....	61
5.2. Tomography approach.....	63
5.2.1. Imaging system.....	63
5.2.2. Experiment.....	64
5.2.3. Results .....	65
5.2.3.1. PA imaging using different number of elements.....	66
5.2.3.2. PA imaging using different size of pixel.....	69
5.3. Summary .....	73
6. Conclusions and future works .....	75
6.1. Conclusions .....	75
6.1.1. Characteristics of transducers .....	75
6.1.2. PA imaging.....	76
6.2. Future works.....	76
Acknowledgement .....	78
References.....	79
국문 요약 .....	88
Appendix.....	91
A.1. Concave transducer.....	91
A.2. Fabrication of transducer .....	91
A.3. Characteristics of transducer.....	93
A.4. PA imaging.....	94
A.5. Summary.....	95

## List of Figures

Fig. 3.1 Structure (a) and photograph (b) of PVDF single element plane transducer.	31
Fig. 3.2 Jig for fabrication of PVDF transducer.	31
Fig. 3.3 Structure of the PMN-PZT transducer.	33
Fig. 3.4 Photograph of the PMN-PZT transducer.	33
Fig. 3.5 Cross section in top view of the PVDF array transducer.	35
Fig. 3.6 Schematic diagram of the CCP pattern.	35
Fig. 3.7 Photograph of the PVDF circular array transducer.	36
Fig. 3.8 Schematic diagram of the PMN-PZT circular array transducer.	37
Fig. 3.9 Photograph of the PMN-PZT circular array transducer.	37
Fig. 4.1 Pulse-echo response measurement system for single element transducers.	39
Fig. 4.2 Pulse-echo response characteristics of the PVDF transducers.	41
Fig. 4.3 Pulse-echo response characteristics of the PMN-PZT hydrophone.	42
Fig. 4.4 Pulse-echo response measurement system for the PVDF circular array transducer.	44
Fig. 4.5 Switch circuit for circuit-array transducer. (a) 120-element circular array transducer, (b) D-sub Screw Terminal Block, (c) LFH160 Connector and (d) Computer with Ni PXI-2576 Connector and LabVIEW software	44
Fig. 4.6 Pulse-echo response characteristics of the PVDF annular-array transducer.	45
Fig. 4.7 Experiment setup of the ultrasound response measurement.	47
Fig. 4.8 Ultrasound signals received by the PVDF and PMN-PZT transducers. (Insertion is the ultrasound signal received by a commercial High Performance PVDF Hydrophone.)	48
Fig. 4.9 Schematic diagram of a PZT transducer (sound source) and the PVDF array transducer.	49
Fig. 4.10 Variation of sensitivity of 120 elements of the PVDF circular array transducer.	51
Fig. 4.11 Variation of sensitivity of 120 elements of the PMN-PZT circular array transducer.	51
Fig. 5.1 Schematic diagram of the deep reflection-mode photoacoustic imaging system. [57]	54

Fig. 5.2 Schematic diagram of the PAM system with single element transducer.....	56
Fig. 5.3 Photograph of the setting details of optical fiber, transducer and SWCNT sample. ....	56
Fig. 5.4 Sample for PA imaging to use the PVDF transducer. ....	58
Fig. 5.5 PA image obtained by the PVDF transducer. ....	58
Fig. 5.6 Sample for PA imaging using PMN-PZT transducer. ....	60
Fig. 5.7 PA images obtained by the PMN-PZT transducer.....	60
Fig. 5.8 Samples for PA imaging in chamber of the PMN-PZT circular array transducer. ....	62
Fig. 5.9 PA image of the sample obtained by scanning acoustic microscopy approach using the PMN-PZT circular array transducer. ....	62
Fig. 5.10 Schematic diagram of a PAT system with linear array transducer. [111].....	63
Fig. 5.11 Scheme diagram of the PAT system with the PMN-PZT circular array transducer. ....	65
Fig. 5.12 Images of the sample obtained by circular array transducer with different number of working element. (a) N=15, (b) N=30, (c) N=60 and (d) N=120.....	68
Fig. 5.13 Images of the sample obtained by the array transducer with different setting size of pixel. (a) a=1.0 mm, (b) a=0.8 mm, (c) a=0.60 mm, (d) a=0.4 mm, (e) a=0.2 mm and (f) a=0.10 mm. ....	72
Fig. 5.14 Images of the sample obtained by circular array transducer when pixel size is 0.5 mm.....	73
Fig. A.1 Structure (a) and photograph (b) of the PVDF single element concave transducer. ....	92
Fig. A.2 Jig for fabrication of the PVDF single element concave transducer .....	92
Fig. A.3 Pulse-echo response characteristics of the PVDF concave transducers. ....	93
Fig. A.4 Ultrasound signals received by the PVDF concave and plane transducers. (Insertion is the ultrasound signal received by a commercial High Performance PVDF Hydrophone.).....	94
Fig. A.5 PA image obtained by the PVDF concave transducer. ....	95

## List of Tables

Table 3.1. Thickness of each layer of the single element PVDF transducer .....	32
Table 3.2 Physical parameters of the matching materials for PMN-PZT hydrophone.	33
Table 4.1 Operational setting of the Pulse-Receiver equipment. ....	40
Table 4.2 Operational setting of the Pulse-Receiver and Pre-Amplifier. ....	47
Table 5.1 Image size of sample changing with the pixel size. ....	73



# **Ultrasound Transducers by Using PVDF and PMN-PZT for Photoacoustic Imaging**

Yonggang Cao

Department of Physics, The Graduate School,

Pukyong National University

## **Abstract**

Photoacoustic (PA) imaging is a new developing imaging modality which has a potential for application in various areas, such as biomedicine and medical diagnosis. This imaging technology is a hybrid modality which combines the high contrast of optical imaging and the high spatial resolution of ultrasound imaging. It is based on the photoacoustic effect of materials or biological tissues, and it uses ultrasound transducers to detect laser-generated ultrasound signals for imaging. In PA imaging systems, ultrasound transducer is a very important part. Various kinds of transducers have been applied in these systems. Most of them are single element, linear array or curved array transducers. Several researchers have used circular array transducers to obtain high resolution images of tissue of small animals. However, the receiving sensitivity of the transducers is still not high enough for detection of weak PA signals.

The aim of this study is to develop the effective ultrasound transducers with high sensitivity in the frequency range of 1~10 MHz which is commonly used for low

frequency PA imaging. In this study, piezoelectric PVDF films have been used to make a plane single element transducers and a 120-element circular array transducer. Besides that, piezoelectric single crystal PMN-PZT has been used to make a needle point transducer (or called needle hydrophone) and a circular array transducer with 120 needle hydrophones.

The pulse-echo response characteristics of the transducers were measured and compared. The results show that the PVDF single element transducer has center frequency about has a center frequency about 10.1 MHz and -6 dB bandwidth about 9.2 MHz (MHz, 91.1% fractional bandwidth). The PVDF circular array transducer has a similar center frequency (11.3 MHz) as the single element transducer. But it has a narrow -6 dB bandwidth about 5.7 MHz (50.4% fractional bandwidth). The PMN-PZT single element and circular array transducer have same center frequency about 6.2 MHz with a -6 dB bandwidth about 5.6 MHz (90.3% fractional bandwidth).

The receiving sensitivities of the fabricated transducers were compared. The PMN-PZT transducer shows a higher receiving sensitivity ( $V_{pp} = 90$  mV) than the PVDF transducer ( $V_{pp} = 50$  mV). The variation of the relative receiving sensitivity of PMN-PZT array transducer is about  $\pm 1.5$  dB. For PVDF array transducer, the relative receiving sensitivity changes in the range from -47.1 dB to -37.9 dB. The PMN-PZT array transducer shows much better uniformity than the PVDF array transducer.

The fabricated transducers were applied to PA imaging systems. The single element transducers were used in a PA imaging system based on scanning acoustic microscopy approach. By comparing the obtained PA signals and PA images, it could be found that the PMN-PZT hydrophone has high PA receiving sensitivity and could

obtained PA images with higher contrast than PVDF transducers. The PMN-PZT circular-array transducer was used in a PA imaging system based on tomography approach. The PA images were obtained with high resolution. Besides that, the influence factors of PAT imaging were discussed.

From this study, it is found that the PMN-PZT hydrophone shows much higher receiving sensitivity than the PVDF transducer. It obtained the PA image with higher quality than PVDF transducer. And the circular array transducer made by 120 PMN-PZT hydrophones can obtain PA images with high contrast. It has the potential to make image with higher resolution.



# 1. Introduction

This chapter gives a background to the imaging modalities in biomedicine. Besides that, the aim and outline of this study are introduced.

## 1.1. Background

Biomedical imaging is a very important method to diagnose and treat human diseases in clinical setting. Based on the development science and technology, people have made enormously progress in imaging technology. Nowadays, imaging technologies include x-ray computed tomography (CT), Ultrasound (US) imaging, magnetic resonance imaging (MRI), single photon emission computed tomography (SPECT), and positron emission tomography (PET). Each of them has its own advantages and disadvantages. Generally, optical and ultrasound imaging modalities are the mostly well-known and widely used ones[1,2].

Optical imaging modalities offer a strong contrast between optically absorption objects. But their penetration depth is poor. Besides that, the high scattering of photons in human body is very harmful. In order to obtain the image with high spatial resolution, the only photons acquired from relatively small penetration depths (microns to a few centimeters) can be used. Common optical imaging techniques include the diffuse optical tomography, optical coherence tomography, angular domain imaging, fluorescence imaging, and near infrared spectroscopy. Other variations of these techniques exist and those all are derived from either the measurement of ballistic or scattered photons. Ballistic photon imaging regimes are those in which photons are not scattered. These photons retain their spatial

information because the net interaction with the object has not perturbed the photon's direction of propagation. Therefore, high resolution optical images can be produced from ballistic photons, but the images are generally limited to approximately a few millimeters in depth of tissues. That is the reason of significantly reducing widespread applicability of this technology.

Ultrasound (frequency over than 20 kHz) imaging is another widely used medical modality. Most of the commercially available ultrasound imaging equipments reconstructs the images by the pulse-echo imaging principle. Pulsed ultrasound waves (approx. 1 to 20 MHz) generated by a transducer transmit into human body through a coupling material. Then the waves interact with tissues, and some of the transmitted energy returns to the transducer and be converted to electric signals. By virtue of signal processing algorithm and technique, the ultrasound image is obtained. The modern ultrasound imaging system works in real-time and gives barely interpretable images. It is noninvasive and doesn't require ionizing radiation. It is the premier imaging modality for soft tissues because of good penetration. By comparing with other modalities such as CT and MRI, ultrasound imaging equipment is compact and portable. But there are also some disadvantages owing to ultrasound. It is almost impossible to propagate through a bone or air, so that the use of it is restricted in brain and lungs. It is also impossible to obtain a diagnostic imaging on the people who are overweight. Another limitation is that its usefulness depends on the skill of the technician or physician performing the examination. The examining results are difficult to reproduce.

Researchers had tried to find an imaging modality which could have the advantages of both optical and ultrasound imaging modalities. In the recent 30 years,

a hybrid imaging modality has attracted a lot of interest. It is called photoacoustic (PA) imaging and combines the advantages of optical imaging and ultrasound imaging. The most drawback of optical imaging is the using of strong photons in human body. Acoustic waves aid in circumventing the issue of optical scatter because ultrasound waves attenuate much less significantly in human tissue ( $\sim 1$  dB/cm/MHz). Characteristic features of the photoacoustic wave are determined by features inherent to the optically absorbent object. This permits optical information to be retrieved from much greater penetration depths (a few centimeters) with resolution comparable to that of US imaging.

PA imaging technology is a developing imaging modality. There are a lot of works to do for the researchers, such as the transducers for PA imaging systems. There are no enough researches about the design and fabrication of the transducers for PA imaging.

## 1.2. Aims and Outline

The aims of this study are to design and fabricate transducers which have high sensitivity and wide bandwidth for high quality PA images. The other aim is to investigate the relation between the characteristics of the transducers and the quality of PA images. This study will be described as following:

In Chapter 2, PA imaging modality is introduced. It contains the basic theory, ordinary imaging systems and classification of the PA imaging.

In Chapter 3, piezoelectric transducers are introduced in advance. Then, two kind piezoelectric materials (PVDF polymer and PMN-PZT single crystal) will be used to

make single element and circular array transducers. The fabrication methods will be introduced in detail.

In Chapter 4, the characteristics (pulse-echo response and receiving sensitivity) of the fabricated transducers are measured. By comparison, the transducers with high sensitivity and wider bandwidth are selected for PA imaging.

In Chapter 5, the selected single element transducers are applied to a PA imaging system based scanning ultrasound microscopy approach. And a circular array transducer is applied in a PA imaging system based on tomography approach. By comparison of the obtained PA images, the relation between characteristics and image qualities are discussed.

In Chapter 6, conclusions are given and future works are listed.

Finally in Appendix, the PVDF single element concave transducer is introduced. It is compared with the plane PVDF transducer in fabrication method, electro-acoustic characteristics and PA imaging.

## 2. Photoacoustic Imaging

### 2.1. PA effect

PA effect is the base of PA imaging technology. The photoacoustic (or optoacoustic) is, in essence, the formation of sound waves following light absorption in a material objects. It was discovered in the 1880s[3]. And it is quantified by measuring the formed sound (pressure changes) with appropriate ultrasound transducers. In photoacoustic effect, an object is excited by low radiation of pulsed optical or RF sources, and generates a sound or stress wave as a consequence of the thermoelastic expansion which is caused by a slight temperature rise (typically less than 0.01 °C), as the results of the energy deposition inside the biological tissue through the absorption of incident electromagnetic (EM) energy. The thermoelastic mechanism has special features that make PA techniques amenable for biomedical applications. First, it does not change the properties of the biological tissue under study. Secondly, only non-ionizing radiation is used, unlike in X-ray imaging or positron-emission tomography (PET). The non-destructive, non-invasive and non-ionizing nature of PA techniques makes them ideal for *in-vivo* applications. Thirdly, the relationships between PA signals and the physical parameters of biological tissues are well defined. This advantage permits the quantification of various physiological parameters such as the oxygenation of hemoglobin.

In soft tissues, the thermal diffusion effect on the PA signal is usually negligible since the EM energy is deposited in the sample within a relatively short time. Therefore, the efficiency of PA generation is high. Upon the absorption of the pulse

energy, the thermal diffusion during the pulse period can be estimated by the following thermal diffusion length:[4]

$$\delta_T = 2\sqrt{D_T\tau_p} \quad (2-1)$$

where  $\tau_p$  is the pulse duration,  $D_T$  is the thermal diffusivity of the sample. Thermal diffusivity for most soft tissues is  $D_T \approx 1.4 \times 10^{-3} \text{ cm}^2/\text{S}$ . For example, for an RF pulse of  $\tau_p = 1.0 \mu\text{s}$ ,  $\delta_T = 0.75 \mu\text{m}$ , which is typically much less than the spatial resolution of most PA imaging systems and the characteristic heating length  $L_p$  defined by the penetration depth of the EM wave or the size of the absorbing structure.

Photoacoustic waves, like all other ultrasonic waves, propagate in three dimensional (3-D) space. For simplicity, the inhomogeneity of acoustic speed in soft tissues is usually neglected in analysis of acoustic wave propagation. The speed of sound is relatively constant at  $1.5 \text{ mm}/\mu\text{s}$  with a small variation of less than 5% in most soft tissues[5]. If acoustic heterogeneity becomes important, we can resort to a pure acoustic imaging technique, such as ultrasound pulse-echo imaging or ultrasound tomography, to map out the acoustic inhomogeneity.

The pressure  $p(r, t)$  at position  $r$  and time  $t$  in a homogeneous liquid-like medium obeys the following wave equation:

$$\nabla^2 p(r, t) - \frac{1}{c^2} \frac{\partial^2 p(r, t)}{\partial t^2} = -\frac{\beta}{C_p} \frac{\partial H(r, t)}{\partial t} \quad (2-2)$$

where  $H(r, t)$  is the heating function defined as the thermal energy deposited by the EM radiation per time per volume ( $c$ : the speed of sound,  $\beta$ : the isobaric volume expansion coefficient,  $C_p$ : the specific heat).

The solution, which is based on Green's function, can be found in the literature of physics or mathematics. In general, the solution of eq. (2-2) in the time domain can be expressed by

$$p(r, t) = \frac{\beta}{4\pi C_p} \iiint \frac{d^3r'}{|r-r'|} \left. \frac{\partial H(r', t')}{\partial t'} \right|_{t' = t - \frac{|r-r'|}{c}} \quad (2-3)$$

The heating function can be written as the product of a spatial absorption function  $A(r)$  and a temporal illumination function  $I(t)$ :

$$H(r, t) = A(r)I(t) \quad (2-4)$$

Particularly, if  $I(t) = \delta(t)$ , the initial photoacoustic pressure at position  $r$  is  $p_0(r) = \Gamma(r)A(r)$ , where  $\Gamma(r)$  is the Grüneisen parameter equal to  $c^2 \beta / C_p$ .

Here, we define the Fourier transform PA imaging on variable  $\bar{t} = ct$  as following:

$$\tilde{F}(k) = \int_{-\infty}^{+\infty} F(\bar{t}) \exp(i k \bar{t}) d\bar{t} \quad (2-5)$$

And

$$F(\bar{t}) = \left(\frac{1}{2\pi}\right) \int_{-\infty}^{+\infty} F(k) \exp(-i k \bar{t}) dk \quad (2-6)$$

where  $k = \omega/c$  and  $\omega$  is an angular frequency and equal to  $2\pi f$ .

Thus eq.(2-6) can be rewritten as:

$$(\nabla^2 + k^2)\tilde{p}(r, k) = ikp_0(r), \quad (2-7)$$

where  $\tilde{p}(r, k)$  is the Fourier transform of  $p(r, \bar{t})$ . Based on Green's theorem, the spectrum  $\tilde{p}(r_0, k)$  of the pressure  $p(r_0, \bar{t})$  detected at  $r_0$  can be written in the frequency domain as:

$$\tilde{p}(r_0, k) = -ik \iiint_V d^3r' \tilde{G}_k^{(out)}(r', r_0) p_0(r'), \quad (2-8)$$

where  $V'$  is the volume of the source  $p_0(r')$ ; and  $\tilde{G}_k^{(out)}(r', r_0)$  is Green's function:

$$\tilde{G}_k^{(out)}(r', r_0) = \frac{\exp(i k |r' - r_0|)}{4\pi |r' - r_0|} \quad (2-9)$$

which corresponds to an outgoing wave.

## 2.2. PA imaging system

An ordinary photoacoustic system usually contains an optical excitation module (laser), an ultrasound measurement module (transducer) and an imaging reconstruction module (signal processing system). The properties of each module affect the quality of PA images. For different objects, choice of the excitation sources and detection transducers might be different.

### 2.2.1. Optical excitation

To obtain a PA image, a short pulsed laser as the excitation source illuminates objects to be measured. Depending on the wavelength, the laser beam penetrates some depth of the objects. In the case of optical excitation, the absorption of laser energy causes a small increase of temperature (approx. less 0.1 K) which is below that of causing physical damage or physiological change to the object. Besides that, it is converted into heat by vibrational and collisional relaxation. This produces an initial pressure increase and subsequent emission of acoustic waves which are detected by an ultrasound transducer. The PA image is then formed by a set of this detected acoustic signals. The initial pressure distribution  $p_0$  is encoded onto this propagation acoustic wave. It can be shown that  $p_0$  at a point  $r$  is proportional to the absorbed optical energy  $H(r)$ [6]

$$p_0(r) = \Gamma H(r) \quad (2-10)$$

where  $\Gamma$  is known as the Grüneisen coefficient, a dimensionless thermodynamic constant that provides a measure of the conversion efficiency of heat energy to pressure and is given by  $\Gamma = \beta c^2 / C_p$  where  $\beta$  is the volume thermal expansivity,  $c$  is the sound speed and  $C_p$  is the specific heat capacity at constant pressure. The absorbed optical energy distribution  $H(r)$  is given by the product of the local absorption coefficient  $\mu_a(r)$  and the optical fluency  $\Phi(r, \mu_a, \mu_s, g)$  where  $\mu_a$  and  $\mu_s$  are the absorption and scattering coefficients over the illuminated tissue volume and  $g$  is the anisotropy factor. Writing  $p_0$  explicitly, we obtain

$$p_0(r) = \Gamma \mu_a(r) \phi(r, \mu_a, \mu_s, g) \quad (2-11)$$

As shown in the eq. (2-11),  $p_0$  depends on several mechanical, thermodynamic and optical parameters. In PA imaging, the mechanical and thermodynamic properties are considered to vary sufficiently weakly between different tissue types that they can be regarded as being spatially invariant. And the PA imaging contrast can be assumed that it is dominated by the optical absorption and scattering properties of object. In fact, it transpires that optical absorption tends to dominate, and for this reason PA images are often described as being 'absorption based'.

The optical absorption coefficient, which is the primary factor for imaging contrast, should be considered firstly in PA imaging experiment. For different objects, the optical absorption coefficients are different. Hemoglobin is the most important organelle in animal blood. It is also known as an effective PA object which has a high optical absorption coefficient below 1000 nm of wave length. The  $\mu_a$  of both oxygenated and deoxygenated hemoglobin at wavelength below 1000 nm is at least

an order of magnitude higher than that of the other chromophores, such as water, lipids and elastin that are present in connective tissues, blood vessels and other organ constituents. Water has a quite different tendency of absorption coefficient that it increases from 400 to 1800 nm.

### 2.2.2. Acoustic detection

Optical-pulse excited pressure acts as an acoustic source for PA imaging. Then the generated acoustic wave propagates in three-dimensional space. Comparing with optical wave, the acoustic wave shows better penetration when it propagates in a biological tissue. For example, the scattering of acoustic wave is less than optical wave. Usually, the attenuation coefficient in a medium is given by following formula:

$$\alpha = af^b \text{ [dB/cm]} \quad (2-12)$$

where  $b$  is a tissue dependent constant,  $1 \leq b \leq 2$  and  $f$  is the frequency expressed in MHz. Many authors consider  $b = 1$ , which is close to reality in many biological tissues[7]. The attenuation coefficients of many soft tissues are nearly about 1 dB/cm/MHz, but it is about 20 dB/cm/MHz for bone (if  $b = 1$ ). The equation shows that the attenuation affects more the higher frequency component and thus acts as a low-pass filter, reducing overall resolution. So that, there is a tradeoff between resolution and penetration depth, which favors lower frequencies which is less attenuated.

Ultrasound velocity in biological tissues is pretty much a constant near 1500 m/s. Except in the highly heterogenous samples, its variation is no more than 10% and usually ignored. These variations of the speed of sound are modeled by acoustic

impedance, which is related to density and sound velocity. Changes in velocity are responsible for reflections at interfaces and refraction. This shows why contrast is usually poor in echography, where reflected sound waves form the signal of interest. Large reflections occur at the interface between the crystal and the tissue, which is why an impedance matching gel is used in echography.

Piezoelectric ultrasound transducers and optical pressure sensors are the most used detectors for PA waves. Although the optical sensors for ultrasound detection are very interesting, it will not be covered in this study. A piezoelectric transducer can detect ultrasound waves and transform the sound signal to electric voltage signal. The amplitude of the voltage signal is proportional to the pressure of the sound wave and the receiving sensitivity of the transducer. The receiving sensitivity  $g$  is the potential produced by a unit strain. The receiving constant  $g$  gives the electric potential difference per unit thickness produced by a unit stress. For a PZT ( $\text{Pb}(\text{ZrTi})\text{O}_3$ ) transducer, the receiving constant is about  $2.5 \times 10^{-2}$  Vm/N. For PVDF (Poly Vinylidene Fluoride) transducer,  $g$  is about five times larger than PZT. Piezoelectric transducer exhibits resonance property, when the wavelength of the generated wave is two times of the piezoelectric element thickness  $L_T$ . And the resonant frequency can be calculated according to the sound velocity  $C_T$  as shown in following:

$$f_T = C_T / 2L_T \quad (2-13)$$

For ultrasound imaging, the most used frequencies are in the range from 1 MHz to 20 MHz. As we know that the pure ultrasound imaging also relies on the detection of acoustic waves. There has been a significantly improvement in this field, and it could be reused for photoacoustic ultrasound detection.

Nowadays, the transducer for ultrasound detection is designed and fabricated with a definite resonant frequency and wide bandwidth. It means that the transducer is sensible to a large range of frequencies around the resonant frequency. For imaging, acoustic waves could be detected by ultrasound transducers in two ways. The first one is using a single transducer and scanning along certain direction in a given geometry (plane, cylinder and sphere). The other is using an array of transducers which don't need a mechanical movement. So that, faster imaging is possible.

### **2.2.3. Reconstruction**

The photoacoustic ultrasound signals detected by the ultrasound transducer are RF pulses. The pulses are Hilbert transformed after rectification to get envelopes of the pulses. The envelopes are digitized and stored on PC in the form of numeric values. It is changed to a PA image by using a reconstruction algorithm. The reconstruction algorithms have been already used in the imaging modalities such as X-ray computed tomography (CT), magnetic resonance imaging (MRI) and ultrasound[5].

Imaging reconstruction is a big challenge for PA imaging. The challenge arises from the factor that the location of the ultrasound source is unknown in the medium. It is called inverse problem. Many different approaches have been suggested to solve this problem. Analytic back-projection algorithm, finite-elements, Radon transform, Fourier domain analysis, diffusion equation base reconstruction are all successful methods[8-13].

### **2.2.4. Development of PA imaging system**

PA imaging system is one of the most interests of photoacoustic research. A

number of groups worldwide have made significant contributions to this topic. It has been developed from the ordinary PA imaging system to photoacoustic microscopy (PAM) and photoacoustic tomography (PAT).

PA and PAM imaging systems are very similar. The difference between these two systems is the center frequency of ultrasound transducers, which is smaller than 30 MHz for PA imaging and larger than 30 MHz for PAM imaging. In both two systems, the transducer is actually analogous to the B-mode scan in ultrasonography. By a mechanical scanner, the PA signals from the sample could be stored respectively. Every detected signal is converted into a 1D image along the acoustic axis of the transducer, analogous to an ultrasonic A-line or A-scan. Then cross sectional images are formed by combining the 1D images acquired from all points. The axial resolution along the acoustic axis depends on both the width of the radiation pulse and the width of the impulse response of the transducer. The lateral resolution is determined by the focal diameter of the ultrasonic transducer.

PA and PAM imaging are the mostly reported methods for PA image. The PAT imaging technology has attracted a lot of interest due to its imaging ability in tens micrometer scale. Kolkman et al.[14] reported an optical-resolution photoacoustic microscopy (OR-PAM) which uses an extreme-narrow aperture sensor to obtain the photoacoustic imaging of blood vessels. The home-built double ring sensor has two concentric equal-area ring-shaped electrodes on one side of piezoelectric element PVDF. It was connected to an amplifier. PA signals were generated by illuminating the tissue through a fiber, which was positioned in the centre of the ultrasound transducer. The images of two joining veins proximal to the wrist of a human volunteer were reconstructed. At depths beyond the optical diffusion limit and up to a

few millimeters, Favazza et al.[15] developed an acoustic-resolution photoacoustic microscopy (AR-PAM) which could achieve high resolution by taking advantage of the much lower acoustic scattering. The AR-PAM system contains a single, broadband, focused ultrasound transducer with 50 MHz central frequency and 70% nominal bandwidth. An optical condenser was set in the optical circuit to focus the laser beam to a diameter of 2 mm in free space at the focal point. And B-scan PA images of human skin were obtained with 15  $\mu\text{m}$  axial and 45  $\mu\text{m}$  lateral resolutions.

Recently, more and more attentions have been paid in reconstruction-based PAT. To accelerate data acquisition, state-of-the-art ultrasonic array detectors have been used for PAT. Zemo et al.[16] introduced a linear array PAT with a multimode optical fiber bundle bifurcated to flank a handheld ultrasonic array transducer. A single laser pulse—with a safe exposure to the tissue ( $\leq 20 \text{ mJ/cm}^2$  in the visible spectral range)—yields a 2-D image. And an ultrasonic imaging system was adapted for current imaging with PAT. A photoacoustic B-scan of subcutaneous micro vessels in a young rat and a surface-rendered photoacoustic image of volumetric data were obtained by this linear array PAT system. The system has the 100  $\mu\text{m}$  lateral resolution, 25  $\mu\text{m}$  axial resolution, and 3 mm imaging depth. Besides that, Li et al.[17] studied the hemodynamics within the entire cerebral cortex of mouse by using a circular array PAT system. The system contains a 5 cm 512-element full-ring ultrasonic array transducer with frequency about 5 MHz which receives PA signals primarily from a slice of 2 mm thickness. It can not only provide 2-D and 3-D imaging of brain vasculature with high resolution.

Several approximated reconstruction algorithms have been demonstrated. Among them, Kruger et al.[18-20] suggested a filtered back-projection algorithm under

circular or spherical measurement geometries, analogous to that used in X-ray computed tomography; Liu[21] presented an approach based on matrix inversion; Hoelen and de Mul et al.[22,23] constructed a time-domain delay-and-sum focused beam-forming algorithm to locate the PA sources in a sample in the planar scan geometry; Köstli et al.[24] reported an image reconstruction by back-projection of detected 2-D pressure distributions; Paltauf et al.[25] studied an iterative reconstruction algorithm to minimize the error between the measured signals and signals calculated from the reconstructed image; and Zhu Lina[26] explored an optimal statistical approach.

Researchers have successfully obtained some PA images of organs of small animals and human, such as the breast and the brain, where the angiogenesis networks, blood vessels, or blood perfusion can be measured. Kruger et al.[18-20] conducted phantom studies and developed TCT scanners with 434 MHz radio waves to image a breast. They acquired images of porcine kidney as well as of human subjects [27-29]. Kruger et al.[30,31] also designed small-animal imaging systems using ultrasound transducer arrays and pulsed laser excitations, and phantom samples as well as nude mice were imaged *ex-vivo*. Katabutov et al.[32] pursued OAT in biological tissues. Esenaliev et al.[33] using a near-IR laser (1064 nm), tested the sensitivity of PAT in detecting small model tumors embedded in bulk phantoms that simulated breast tissues. Oraevsky et al.[34] applied an arc array to the detection of breast cancer *in-vivo*. Hoelen et al.[23] demonstrated that PAT can image blood vessels with high resolution *ex-vivo*. Wang et al.[35] tested tissue phantom samples in various measurement geometries using both laser and RF excitations. They reported the first *in-vivo* noninvasive transdermal and transcranial imaging of the structure and

function of the rat brain by means of laser-induced PAT and then successfully demonstrated 3-D imaging[36,37]. In addition, an optical method was demonstrated for 2-D ultrasonic detection[12,24,38-40]; and a material that may be suitable as a breast phantom for use in photoacoustic imaging was also reported[41].

A recent breakthrough in PAT research is the exact reconstruction theories. Xu et al.[42,43] reported exact Fourier-domain reconstructions for spherical and cylindrical measurement geometries with point-detector measurements. Both Xu and Köstli et al.[38,44,45] presented an exact Fourier-domain reconstruction for planar scans. Xu et al.[42,46] also demonstrated that exact Fourier-domain reconstructions can be closely approximated by time-domain modified back-projection formulas with spatial weighting factors, which are the cosines of the angles between the normal of the detection surface and the vectors from the detection positions to the reconstructed points of the acoustic sources. These works clearly revealed the degree of approximation between the exact solutions and the approximate back-projection methods including those reported by other researchers.

### **2.3. Classification of PA imaging**

With the development of optical and ultrasonic technology, there are more and more PA imaging systems are introduced. Generally, there are three approaches for PA imaging.

#### **2.3.1. 2-D PA imaging**

A 2-D photoacoustic imaging system is widely used because it is a relatively simple and inexpensive way to produce comparatively high resolution PA images.

The system employs the use of a single transducer that is mechanically scanned around the perimeter of a sample. At the predetermined transducer location, the PA signal is recorded, and then the transducer scans by a given angle. The universal back projection algorithm is used to reconstruct a 2-D image. This system has been successfully used to visualize light-absorbing objects, including vasculature in the mouse brain[24,37], peripheral joints in humans[47] and many others. It has been used to measure fluorescent agents[48], to characterize hypoxia in mouse brain[49], and to monitor angiogenic vascular growth in mouse[50]. Because this system only uses a single transducer and single acquisition channel, it is relatively inexpensive and simple to construct. However, the system suffers from relatively long data acquisition times due to the mechanical scanning of a single transducer. As well, images are localized to the selected plane and, therefore, translation to 3-D images is not possible without scanning the object or transducer to produce images of multiple 2-D planes.

Another design, called light-induced optoacoustic imaging system (LOIS) was developed by Oraevsky et al.[51], in order to image and diagnose breast tumors. In various generations, the system utilizes a curved array of transducers with 32, 64, or 128 channels. The array is designed with very high focus in the selected imaging plane but extremely directional sensitivity elsewhere. Therefore, a slice of the breast can be selected. The sensitivity of the system to detect breast tumors is compared to other imaging modalities, where it was recently shown to have higher sensitivity than x-ray mammography but lower than ultrasound. The system can display images at relatively high frame rate (1-10 Hz) but suffers from high cost associated with the transducer count and data acquisition channels utilized. Of course, this system is also

limited to producing only 2-D images.

In 2008, Zemp et al.[52], introduced a high frequency photoacoustic microscopy (PAM) system capable of producing 2-D images in real-time. The system consists of a high-repetition rate laser and an ultrasound array with peak detection at 30 MHz. The entire imaging process, from data acquisition to image display, is produced at 50 fps. The system has been used to image a variety of phantoms as well as *in-vivo* absorbing structures at depths around 3 mm.

### **2.3.2. 3-D PA imaging**

Photoacoustic microscopy utilizes a highly focused, high frequency transducer that is scanned across the sample. Because the transducer is highly focused, each PA measurement recorded is well localized. 3-D images are then rendered by stacking the PA line scans that are garnered from sequential scanning. This technique produces high resolution images at depths much greater than conventional microscopy. PAM has been used broadly for a variety of applications to produce 3-D PA images. Examples include imaging skin melanoma[53], vasculature features[54-56], skin burns[57], and has been recently integrated with OCT to do simultaneous multimodal imaging[58].

An etalon scanner has been developed, to produce 3-D PA images. In this scheme, a thin film acts as a Fabry-Perot etalon[59-61]. The acoustic pressure causes slight changes in the film thickness and can be probed by a laser to quantify these changes. This approach acquires the pressure measurements in a 2-D plane, which are then reconstructed into a 3-D volume using a Fourier transform algorithm. This detection scheme produces images of relatively high resolution and contrast but suffers from

limited penetration depth and slow image acquisition times.

Carson et al.[62], implemented a system similar to the PAT system developed by Wang[37]. In this system, a single transducer is stepped around an object within a single plane. By applying the universal back projection algorithm, tomographic images are produced. In order to generate 3-D images, the PA signals must be collected along the surface of a sphere. This concept was applied by scanning the transducer along an arc in which a relatively large solid angle was covered. This was utilized to image animal joints with resolution of a few hundred micrometers[63].

Kruger et al.[20] developed a method using a hemispherical array of transducers with a directional sensitivity overlapping at the centre of the hemisphere, but using thermoacoustic principles. This method employs the use of a radio frequency (RF) antenna, emitting waves at 434 MHz directed towards the centre of the hemisphere. The hemisphere is rotated, and at each position, the RF pulse is absorbed by the PA source where the transducers can sample the PA wave. Once data is acquired over 360°, a Radon transform reconstruction algorithm is utilized to produce 3-D images. While the implementation and detection scheme is similar to the realization employed in our system, a significant difference is the mechanical scanning utilized by Kruger et al.[20] to acquire data, greatly increasing the time required to produce a single 3-D image.

Paltauf et al.[46] have done significant research producing PA images using integrating line transducers. This has been used to generate 2-D images, and with modifications to the reconstruction technique, has produced 3-D images as well. These transducers are organized so that they satisfy the 2-D wave equation and

therefore, measured data can be used to produce images by temporal back projection algorithms. This technique has been used to represent a variety of phantom objects[64,65].

A group of the University of Twente has integrated a light delivery system with a disc-shaped piezoelectric transducer[66]. The optical fibers are situated at the side of the transducer where reflection mode imaging is used. In this particular realization, weighted delay-and-sum reconstruction was used to produce 3-D maximum intensity projection images of the PA source distribution. This was firstly used to image neovascularization in tumor angiogenesis in rats[67].

### **2.3.3. Real-time PA imaging**

Real-time imaging is vital in viewing dynamic processes. As mentioned earlier, Zemp et al.[52,68] produced real-time 2-D images of cardiovascular dynamics in a mouse at 50 fps by using a beam-forming technique and a 48-channel array. Niederhauser et al.[40,69] also demonstrated real-time imaging at 7.5 fps of human vasculature in a 64-channel array. Most recently, Gamelin et al.[70] produced a 512-element curved transducer array (parallel channel acquisition) to produce tomographic images of small animals at 8 fps. Other PA analysis has been done in real-time, including real-time flow cytometry[71]. However, the extension to real-time 3-D images is not trivial as the 2-D real-time techniques would require scanning the transducer array to transition to the 3-D regime.

A 3-D real-time technique was developed by Song et al.[72], producing 3-D PA images of mouse vasculature at 3 seconds per frame. The system scanned the transducer array over the mouse skin while employing a laser with 1 kHz repetition

rate. The 996 nm laser pulses were used to produce a single 3-D image. While this was a significant technological advancement, multiple laser shots were utilized to produce a single 3-D image, diminishing the effective temporal resolution of the system. Ideally, a system would utilize a single laser pulse to produce a 3-D PA image such that each 3-D frame represents a snap-shot of the PA source over the interval of the lasers pulse duration (5~10 ns).

## 2.4. Influence factors on PA imaging

For obtaining PA imaging of an object, the ultrasound signals which are excited by pulsed laser are influenced by the structure and optical property of the object. The ultrasound signals are collected and used to reconstruct the PA imaging of the object. The resolution of reconstructed imaging is affected by following factors.

(1) Pulse duration of laser: To avoid the thermal relaxation after optical excitation, the pulse duration of laser should be short. Under this condition if the duration is longer, the higher energy of single pulse is obtained and the examination depth is larger. But the resolution of the imaging will be reduced.

(2) Frequency of ultrasound signal: The ultrasound frequency is determined by the volume of the object. Usually, the object with small volume generates high frequency ultrasound signals. However, the ultrasound attenuation has a functional relationship to frequency. The increase of frequency causes a high attenuation and a decrease of examination depth. Because the bandwidth of ultrasound transducer is usually in a limited region, the resolution of imaging is mainly determined by the bandwidth of transducer.

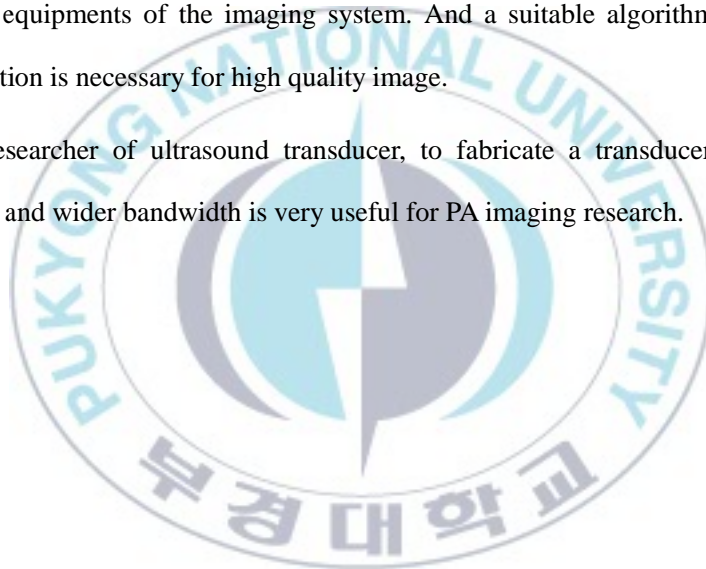
(3) Sensitivity of the ultrasound transducer: During the propagation of ultrasound signal, the inner signal becomes very weak due to attenuation. So that transducer with high sensitivity is possible to detect the weak ultrasound signals.

(4) Algorithm: The reconstruction algorithm affects the resolution of imaging.

## 2.5. Summary

For PA imaging, the pulsed lasers and ultrasound transducers are the most important equipments of the imaging system. And a suitable algorithm for image reconstruction is necessary for high quality image.

As a researcher of ultrasound transducer, to fabricate a transducer with high sensitivity and wider bandwidth is very useful for PA imaging research.



### **3. Piezoelectric transducers for PA imaging**

To fabricate a transducer with high receiving sensitivity and wide bandwidth for PA imaging, the piezoelectric transducers are classified firstly. Piezoelectric materials which have the potential for high sensitivity and wide bandwidth are introduced to make single element and circular array transducers.

#### **3.1. Piezoelectric transducers and PA imaging applications**

##### **3.1.1. Polymer transducer**

In 1948, Ford and Hanford[73] patented polyvinylidene fluoride (PVDF). Thereafter, Professor Heiji Kawai and his former research colleague Dr. Eichii Fukada of the Kobayasi Institute of Physical Research in Tokyo did a plenty of work on piezoelectricity in organic materials. In 1969, they reported the discovery of a large remanent polarization in the oriented films of PVDF. Since then, many new piezoelectric and ferroelectric polymers materials have been studied in great detail, such as polyvinylidene fluoride-trifluoroethylene (P(VDF-TrFE)), polyvinylidene fluoride-tetrafluoroethylene P(VDF-TeFE) and nylons[74-76]. Among them, PVDF and P(VDF-TrFE) are the most widely used piezoelectric polymers.

Piezoelectric polymers are so flexible that they could be used to make transducers in various shapes, such as curved array and concave array. And it is easy to obtain very thin (several micrometer) piezoelectric polymer films for making high or

ultra-high frequency transducers. Besides that, they have low density, low acoustic impedance, and relatively high piezoelectric constants. There are several disadvantages of the polymers, which limit the widely applications of them. The weak piezoelectric property negates the possibility of polymers for high power transducers. Besides that, the stability of polymer is also a limitation.

Piezoelectric polymers have been well known as the suitable materials for making calibration hydrophones, extremely broadband acoustic transducers, and specialized contact transducers[77-80]. And the low acoustic impedance and high mechanical flexibility make it an attractive material for the construction medical transducers. Ohigashi et al. obtained the pulse echo image by using 13 mm diameter, 5 MHz single element PVDF transducer[81]. Foster et al. made a 13 MHz polymer transducer which was applied in the study of breast tissue specimens.

Piezoelectric polymers show the absolute advantage in high frequency transducer above 15 MHz for medical and biological imaging. Jeong et al. made disk-type and ring-type P(VDF-TrFE) transducers with center frequency 23 MHz [-6 dB bandwidth 102%] and 20 MHz [-6 dB bandwidth 103%][82]. Both two transducers are successfully applied for sectional scan (B-mode) of a wire phantom for prototype. Ketterling et al.[83] reported their design and fabrication of a 36 MHz 5-element PVDF annular array transducer. And the insertion losses (ILs) for the matched annuli ranged from 28 to 38 dB. The transducer was successfully used for utero imaging of mouse embryos[84,85]. Carey et al.[85] designed and fabricated a 20 MHz, 128-element PVDF linear array transducer. The imaging test shows that the system with the transducer has an axial resolution about 40  $\mu\text{m}$  and a lateral resolution about 0.2 mm.

Due to the advantages in high frequency and wide bandwidth, the piezoelectric polymer transducers were usually used for PA imaging. Hoelen et al.[22] reported the simulation works of PA image reconstruction assuming a 9  $\mu\text{m}$  thick PVDF transducer was used in experiment. Also, three needle hydrophones (Precision Acoustics Ltd.) with an active PVDF piezoelectric element with effective diameters of 75, 200 and 500  $\mu\text{m}$  were used and compared in experiment of PA imaging. Huang et al.[86] used nanoimprinting technique to make a polymer microring resonators for low-noise, wideband ultrasound detection in PA imaging. Fung et al.[87] used a PVDF transducer for detection of the thermal waves (PA signals). The results show that the PVDF transducer is very effective in detecting the normal to superconducting samples at low temperatures such as thermal diffusivity, thermal conductivity and the specific heat capacity. Zhang et al.[60] successfully obtained high-resolution 3-D photoacoustic imaging of superficial vascular anatomy by using a Fabry–Perot polymer film ultrasound sensor.

### 3.1.2. Single crystal transducer

Quartz is one of the most widely known piezoelectric single crystals. It has very large mechanical quality factor ( $Q_m = 2 \times 10^6$ ), while the electromechanical coupling coefficient is much smaller ( $k_t = 0.093$ ) than the one generally used in recent years. Piezoelectric thin quartz was used to make the first transducer in the 1<sup>st</sup> World War. Normally, it is widely used for ultrasound filter due to its good stability. Edward et al.[88] made a digital pressure transducer utilizing a precision 5 MHz piezoelectric quartz resonator. Zhang et al.[89] reported a novel piezoelectric quartz micro-array immunosensor. The quartz oscillator or resonator was first developed by Walter

Guyton Cady in 1921[90]. George Washington Pierce designed and patented quartz crystal oscillators in 1923[91]. Due to the characteristic of quartz (such as, very high quality factor  $Q_m$  and very small electromechanical coupling coefficient  $k_t$ ), it is not suitable for making broadband and sensitive transducer for medical imaging.

Single crystals such as  $\text{Pb}(\text{Mg}_{1/3}\text{Nb}_{2/3})\text{O}_3\text{-PbTiO}_3$  [PMN-PT] and  $\text{PbZrO}_3\text{TiO}_3\text{-PbTiO}_3$  [PZT-PT], are recently synthesized artificial materials with piezoelectricity. The dielectric and pyroelectric properties of single crystal PMN-PT have been reported in 1989[92]. PMN-PT have been found to exhibit longitudinal coupling coefficients  $k_{33} > 90\%$ , dielectric constants ranging from 1000 to 5000 with low dielectric loss  $< 1\%$ , and exceptional piezoelectric coefficients  $d_{33} > 2000$  pC/N. Many researchers have studied PMN-PT single crystal for medical applications[93]. They use it to make transducers which have wide bandwidth, efficient emission and sensitive receiving characteristics. Saitoh et al.[94] made a phased array transducer using PZN-9%PT single crystal with the center frequency about 3.7 MHz. The transducer had 5 dB more sensitivity and 25% more fractional bandwidth at  $-6$  dB than the conventional PZT array. A PZN-PT single crystal composite transducer was made with a  $-6$  dB fractional bandwidth of 100% in 1-3 structure, and a PMN-PT transducer with a fractional bandwidth of 114%[95]. Ritter et al.[96] reported single element PZN-PT composite transducer with a fractional bandwidth of 75–141%. Base on the reported achievements on PMN-PT research, Philips[93] has realized the commercial application of PMN-PT single crystal transducer for cardiac harmonic imaging. Zhou et al.[97] used a poled PMN-PT single crystal (50  $\mu\text{m}$  thickness and 0.4 mm  $\times$  0.4 mm area) to make an ultrasonic needle hydrophone with one matching layer. The centre frequency and  $-6$  dB fractional bandwidth of the hydrophone were

44 MHz and 45%, respectively. The two-way insertion loss was about 15 dB. The hydrophone was used to obtain *in-vivo* high-frequency, pulse-wave Doppler pattern of blood flow in the posterior portion and ultrasonic backscatter microscope (UBM) image of rabbit eye.

Due to high electromechanical coupling factor and piezoelectric constants, single crystals have attracted a lot of interests for application of transducers to PA imaging systems. Yang et al.[98] developed a 2.5 mm outer diameter photoacoustic endoscopic mini-probe to use in the instrument channel (typically 2.8 or 3.7 mm in diameter) of standard video endoscopes. In the probe, a focused ultrasonic transducer was fabricated by using a highly-sensitive PMN-PT piezoelectric material. Li et al.[99] used 35 and 80 MHz PMN-PT ultrasound transducers in catheter-based intravascular photoacoustic (IVPA) imaging system and obtained the PA images with high resolution. Jansen et al.[100] designed and fabricated a PMN-PT transducer. The transducer has center frequency about 44.5 MHz and -6 dB fractional bandwidth about 45%. The PA imaging system by using this transducer has demonstrated successfully for lipid detection in an atherosclerotic human coronary artery.

It could be found that PMN-PT piezoelectric single crystal ultrasound transducer is usually used in PA imaging system. It is hard to find reports about PMN-PZT piezoelectric single crystal, even it has higher electromechanical coupling factor and piezoelectric constants.

### **3.1.3. Ceramic transducer**

Piezoelectric ceramic is a poly-crystal ferroelectric material with high dielectric constants. Its good piezoelectric properties were found during the studies on Barium

Oxide-Titanium ( $\text{BaTiO}_3$ ) between 1941 and 1947. After  $\text{BaTiO}_3$ , Lead Niobate ( $\text{PbNbO}_3$ ) was discovered by Goodman in 1952. And later in 1954, Lead Zirconate Titanate (PZT) was found by Jaffe et al.[101] The discovery of piezoelectricity of PZT marked a milestone in the development of piezoelectric ceramics because of its strong and stable piezoelectric characteristics and its wide range of operating parameters. Although many other assimilable ceramics were discovered later [such as Lead Titanate (PT), Lead Metaniobate (PN) and Lead-Barium Lithium Niobate (PBLN)], PZT and related materials (PZT with various additives) have constituted the domain piezo-ceramics in ultrasonic applications in the last 50 years.

Among various piezoelectric ceramic materials, PZT is mostly chosen for making transducers. Piezoelectric PZT is commercially available in various structures, such as disk, ring, and tube and so on. It is very convenient to make single element transducers by using those commercial PZT elements. Nowadays, it is interesting to make PZT transducers with high/very-high center frequency, high sensitivity and efficiency. Yamaguchi et al.[102] made the PZT films with 0.22 to 2.56  $\mu\text{m}$  thickness by sol gel method. The minimum conversion loss obtained was less than 3.8 dB at 1.75 GHz. And Lukacs et al.[103] made a composite ultrasound transducer by using sol gel method. The fabricated single element focusing transducer had been produced that operate in the frequency range of 70 MHz to 160 MHz with a -6 dB bandwidth up to 52%. The images of phantom materials and *ex-vivo* biological samples were obtained by this transducer. PZT is also widely used to make various array transducers. Usually, PZT arrays are manufactured from PZT blocks which are divided into elements using a diamond wire saw. Foster et al.[104] made a PZT linear array transducer with 256 elements which were obtained from a PZT block by laser

cuts. The transducer had the bandwidth of high-performance ultrasound imaging from 15-50 MHz. By using high-frequency micro-ultrasound system with this transducer, it is possible to obtain real-time color and power Doppler images of biological samples. PZT composite transducer is also a kind of array transducer. It is made by combining unconnected PZT elements with a passive polymer phase[105]. There are ten connections between PZT and polymer, such as 0-0, 1-0, 2-0, 3-1 and so on[106]. It is possible to improve the sensitivity and efficiency of the transducers. For example, the 3-1 composite made by PZT and epoxy cement has a large voltage coefficient. And 2-2 composite has been produced for filters and other high-frequency applications.

As one of the mostly used piezoelectric transducer, PZT transducers are also used in PA imaging system. Some researchers directly used the US imaging PZT transducers for PA imaging. Zhao et al.[107] used a PZT transducer to detect the PA signals from weakly absorbing liquids. Some researchers also designed and fabricated a PZT transducer for PA imaging. Xi et al. used a designed 5.5 MHz unfocused ring shape PZT transducer in an intraoperative PAT system and obtained 3-D tumor mapping in a mouse model.

Generally speaking, piezoelectric ceramics have strong piezoelectricity with high dielectric constants, and can be cut into varies size and shape, but their small mechanical quality factors, high electric loss and poor stability are the disadvantages.

### **3.2. Transducer fabrication for PA imaging**

As introduced in Section 3.1, the transducer for PA signal detection should have high sensitivity and wide bandwidth. So, there are more requirements of the piezoelectric materials.

In this study, piezoelectric polymer PVDF and single crystal PMN-PZT were selected to make the transducers for PA imaging. The former one is the mostly used for wide bandwidth transducer, such as a hydrophone. The latter, which has higher electromechanical coupling factor and piezoelectric constants with high permittivity and low dielectric loss, is an ideal piezoelectric material for making high receiving sensitivity transducer. And two kind materials are used to make two kind transducers, single element and the circular array transducers. The thicknesses of PVDF and PMN-PZT are commercial available 28 and 310  $\mu\text{m}$ .

### **3.2.1. Single element transducers**

#### **3.2.1.1. PVDF transducer**

Figure 3.1 shows the structure and photograph of the PVDF single element transducer. As shown in Fig. 3.1 (a), the transducer has a 28  $\mu\text{m}$  piezoelectric PVDF film with an Ag electrode on one side, and a copper-clad polyimide (CCP) film bonded with the PVDF film by epoxy (EPO-TEK 301) as another electrode of the transducer. The PVDF transducer was caged by a steel case with a BNC connector. The CCP electrode is connected with BNC (+) by a wire. And Ag electrode was connected with BNC (-) by silver ink. The empty space of the case was filled with the Epoxy (EPO-TEK 301) as backing material. The photograph of the fabricated PVDF transducer is shown in Fig. 3.1(b). The thicknesses of the materials for making transducer are shown in Table 3.1.

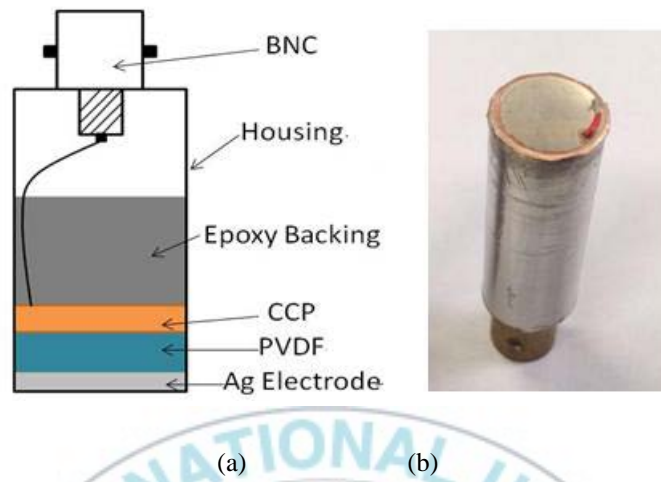


Fig. 3.1 Structure (a) and photograph (b) of PVDF single element plane transducer.

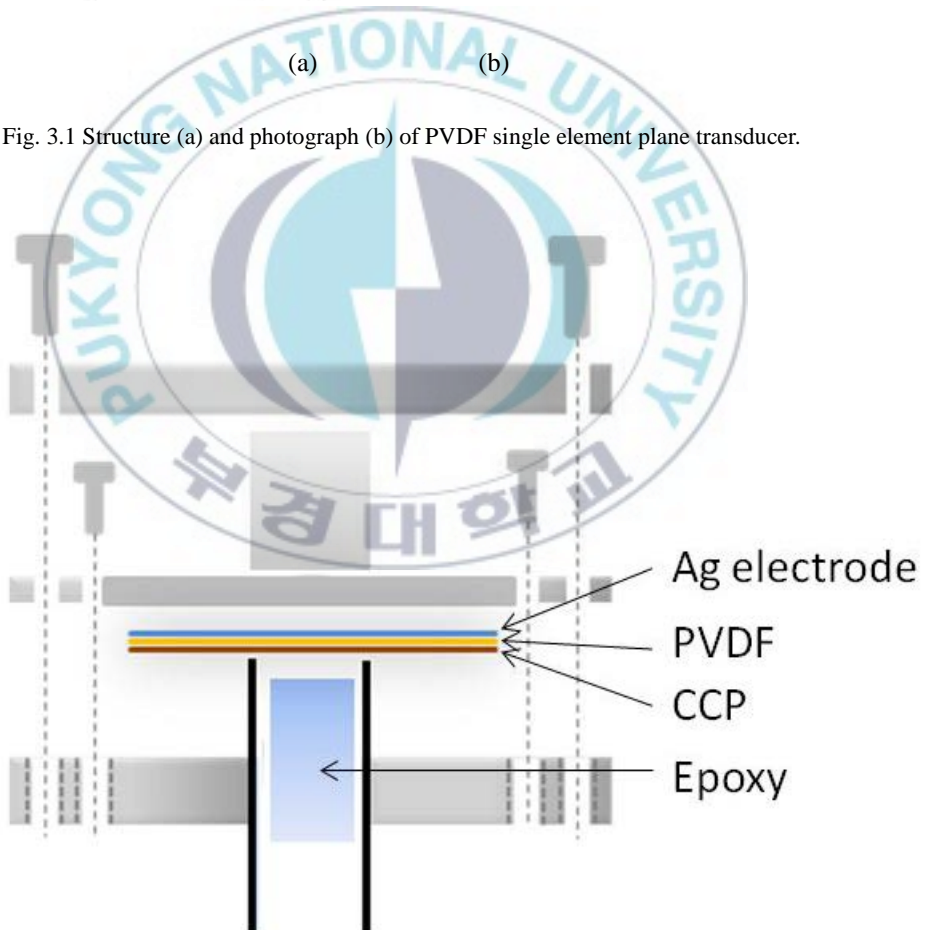


Fig. 3.2 Jig for fabrication of PVDF transducer.

Table 3.1. Thickness of each layer of the single element PVDF transducer

Element	Name	Thickness
Piezoelectric Materials	PVDF	28 $\mu\text{m}$
Upper Electrode (-)	Silver	3~4 $\mu\text{m}$
Under Electrode (+)	Copper-clad polyimide	18 $\mu\text{m}$
Backing Block	EPO-TEK 301	--
Bonding	EPO-TEK 301	--

The transducer was fabricated by using a pressure jig, which was used for the bonding of each element of the transducers. Figure 3.2 shows the jig for making the plane transducer. Suitable pressure was applied to the jig by a hydraulic press (SSP-10A, Shimadzu), so that each layer could be bonded tightly.

### 3.2.1.2. PMN-PZT transducer

Figure 2.3 depicts the structure of the PMN-PZT single element transducer (needle hydrophone). A Cu wire ( $\Phi \approx 0.7 \text{ mm}$ ) was bonded with a 310  $\mu\text{m}$  thick and  $0.5 \times 0.5 \text{ mm}^2$  area PMN-PZT plate (Ceracomp Co. Ltd.), which has piezoelectric coupling coefficient  $k_{33} \approx 0.92$  and  $\epsilon_{33}^s \approx 1030$ , by using a conductive sliver epoxy (EPO-TEK H20). The wire was coated by Teflon and inserted into a stainless steel tube. Non-conductive epoxy (EPO-TEK 301) filled around the PMN-PZT for insulation and watertight. The upside electrode were connected to the tube by a gold line which was made by a sputtering system. In addition, matching layer 1 & 2 were attached with the PMN-PZT by non-conductive epoxy (EPO-TEK 301) tightly. Two matching materials were composites ones of epoxy and metal powder, which were supplied from a company (Mico Co. Ltd.). The photograph of the fabricated

PMN-PZT needle hydrophone is shown in Fig. 3.4. Table 3.2 shows the physical parameters of the two matching materials for the PMN-PZT hydrophone.

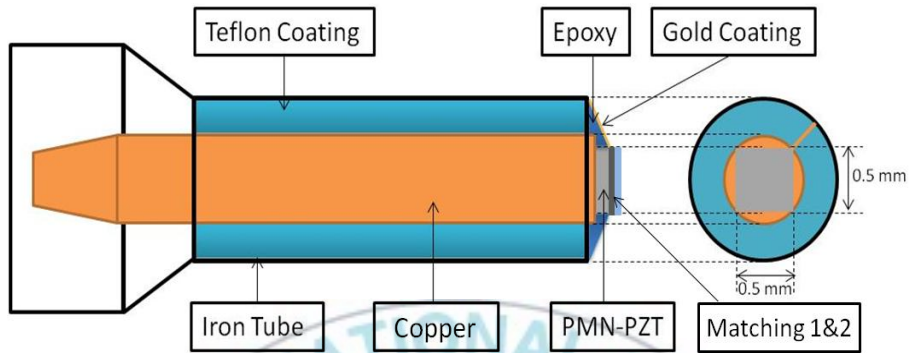


Fig. 3.3 Structure of the PMN-PZT transducer.

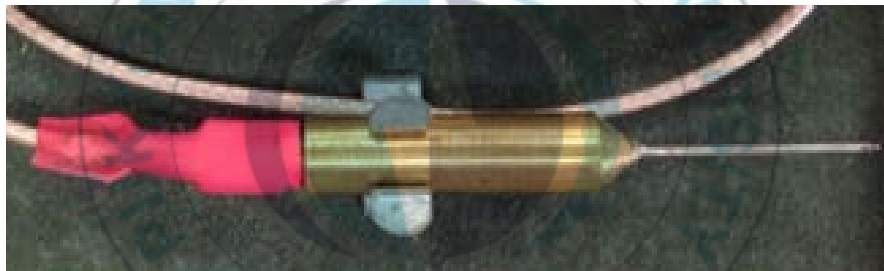


Fig. 3.4 Photograph of the PMN-PZT transducer.

Table 3.2 Physical parameters of the matching materials for PMN-PZT hydrophone.

Parameters	1st matching	2nd matching
Longitudinal Velocity [m/s]	2375.0	2015.0
Density [ $\text{kg/m}^3$ ]	3621.0	1413.0
Impedance [MRayls]	8.6	2.9
Loss [dB/cm, 5 MHz]	20.8	40.0
Thickness [ $\mu\text{m}$ ]	63.0	50.0

## 3.2.2. Circular array transducers

Two kinds of circular array transducers were designed and fabricated in this paper. The two transducers were fabricated by using different materials and different processes.

### 3.2.2.1. PVDF transducer

Figure 3.5 shows the cross section in top view of the PVDF circular array transducer. The radius of circular fluid chamber is 19 mm. The array transducer was assembled by three parts. Each part has 40 elements. The active acoustic component of the transducer was a 28  $\mu\text{m}$  piezoelectric PVDF film with Ag electrode on front-side. The array elements were formed on a CCP pattern which was bonded to back-side of PVDF film using epoxy (EPO-REK 301). And then the (PVDF+CCP) film was bonded to acryl blocks with circle arc of  $120^\circ$ . It is convenient to measure the pulse-echo properties and ultrasound receiving properties of the 40-element array transducers before they were combined.

The electrode-pattern on the CCP was made by using standard copper etching techniques. Figure 3.6 shows the schematic diagram of the pattern. There are 120 (40 $\times$ 3) array elements. The size of each element is  $10\times 0.7\text{ mm}^2$ . Between two elements, there is a 0.3 mm wide kerf. All array elements have extended lead lines which will be connected to the electrical connection pads. The photograph of the fabricated PVDF circular array transducer is shown in Fig. 3.7.

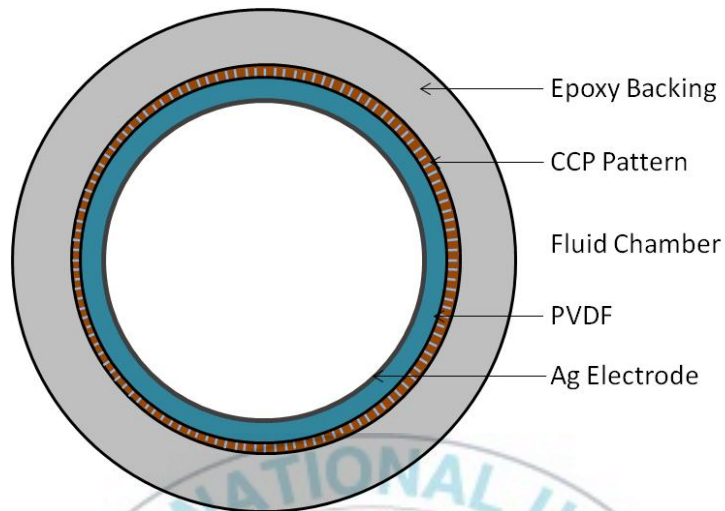


Fig. 3.5 Cross section in top view of the PVDF array transducer.

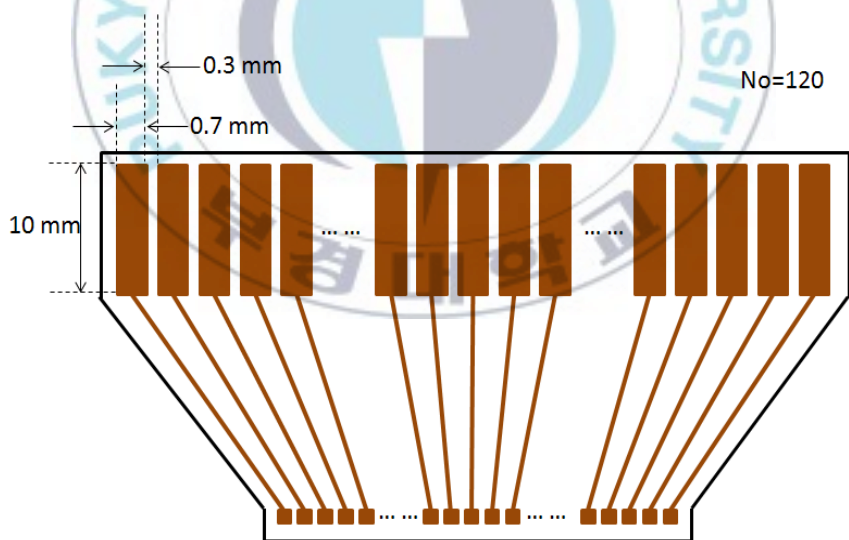


Fig. 3.6 Schematic diagram of the CCP pattern.

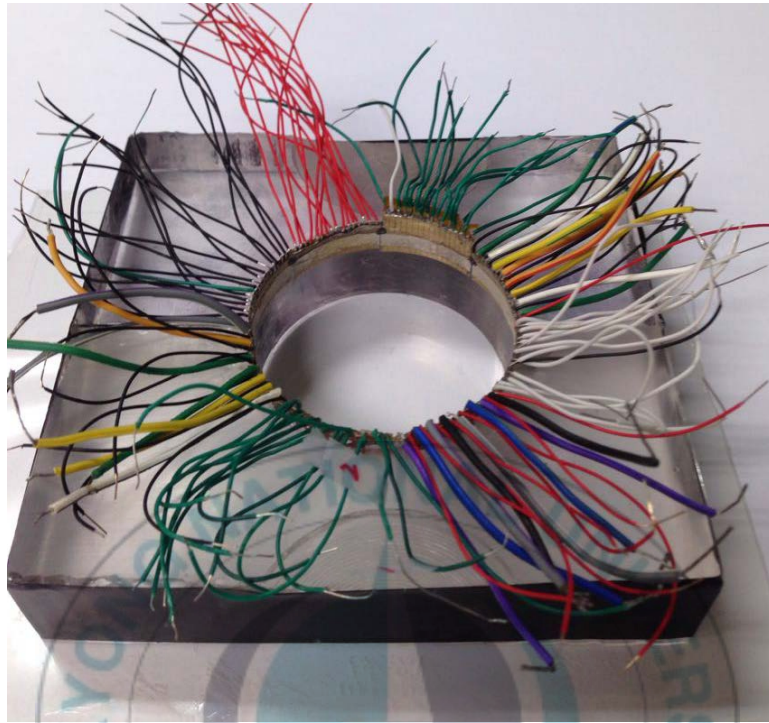


Fig. 3.7 Photograph of the PVDF circular array transducer.

### 3.2.2.2. PMN-PZT transducer

Figure 3.8 shows the schematic diagram of the PMN-PT circular array transducer, which contains 120 PMN-PT hydrophones. These hydrophones are as the same as the PMN-PZT hydrophone which has been introduced in Section 3.2.1.2. All hydrophones were fixed on a plastic base ( $D = 50$  mm) which has 120 channels for the hydrophones. The horizontal channels point to the center of the fluid chamber. The angle between every two neighbor hydrophones is  $3^\circ$ . The photograph of the fabricated PMN-PZT circular array transducer is shown in Fig. 3.9.

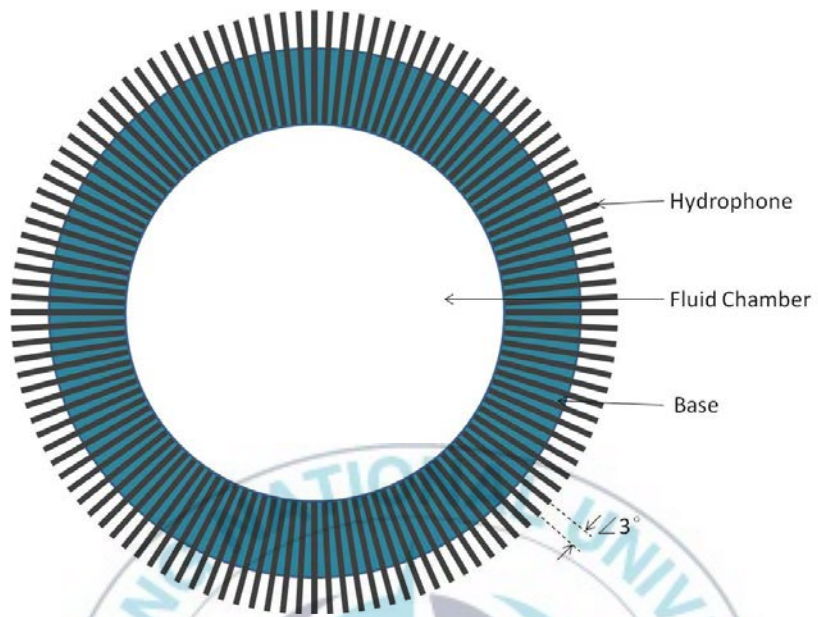


Fig. 3.8 Schematic diagram of the PMN-PZT circular array transducer.

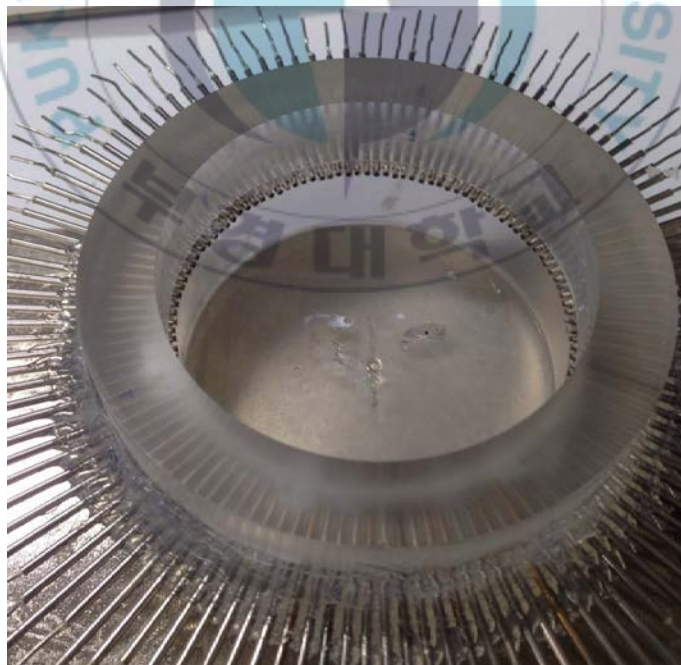


Fig. 3.9 Photograph of the PMN-PZT circular array transducer.

### 3.3. Summary

In this chapter, three kinds of transducers were introduced. Piezoelectric polymers are well known as the suitable materials for making transducer for ultrasound receiving. And some piezoelectric single crystals show the potential for making transducer with high receiving sensitivity due to their high electromechanical coupling factor and piezoelectric constants. Two available piezoelectric materials, 28  $\mu\text{m}$  thickness PVDF polymer and 310  $\mu\text{m}$  thickness PMN-PZT single crystal, were used to fabricate single element and circular array transducers in this study.

For making the PVDF single element transducer, CCP film was used as the backside electrode. And the backing material was epoxy. The PVDF circular array transducer has the similar structure as the single element transducer. But the CCP film was a 120-element pattern. The PMN-PZT hydrophone was fabricated by bonding PMN-PZT plate with a Cu backing material. Besides that, two matching layers were used for improvement of receiving sensitivity and bandwidth. The PMN-PZT array transducer was fabricated by 120 PMN-PZT hydrophones.

Before applying them to PA imaging systems, their electro-acoustic characteristics will be measured and compared. The results will be described in the next chapter.

## 4. Characteristics of the fabricated transducers

To evaluate the ultrasound radiating and receiving characteristics of the fabricated transducers, pulse-echo response and receiving sensitivity were measured.

### 4.1. Pulse-echo response

The pulse-echo method is a very useful technique for nondestructive testing. It could be used to measure the velocity, wavelength and attenuation coefficient (damping constant) of acoustic wave. It is also a useful method to evaluate the characteristics of ultrasound transducer.

#### 4.1.1. Single element transducers

##### 4.1.1.1. Experiments

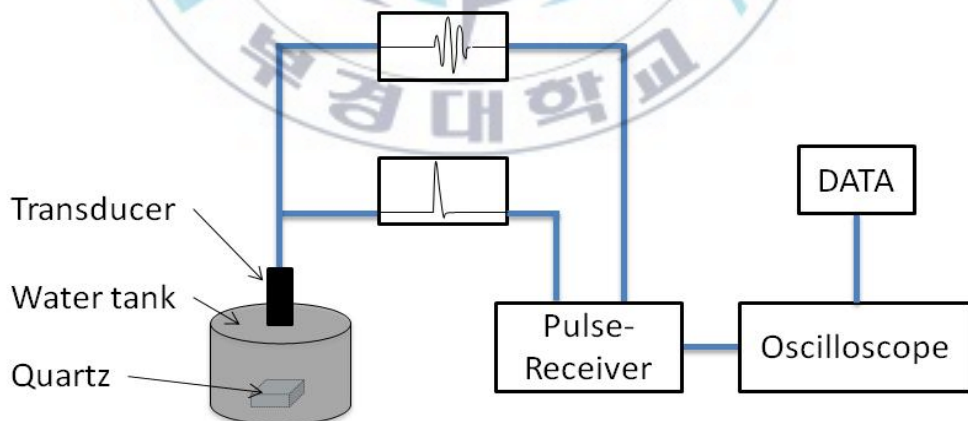


Fig. 4.1 Pulse-echo response measurement system for single element transducers.

Figure 4.1 shows the pulse-echo response measurement system for single element

transducers. A transducer was set in a water tank where there was a quartz target for sound wave reflection. The transducer was excited by an electrical pulse signal which was generated by Pulse-Receiver equipment (MKCNDT XTR- 2020, MKC Korea). And the reflected ultrasound signal was also received by the Pulse-Receiver equipment. By using a digital storage oscilloscope (LeCroy LT322, Chestnut Ridge, NY) with a wave-processing package, the ultrasound signal was viewed and stored. During testing, the transducer was fixed by an iron stand. The head of transducer was inserted into water. The transducer was connected with the Pulse-Receiver by a cable with BNC connector. Table 4.1 shows setting parameters of the Pulse-Receiver for pulse-echo response measurement of single element transducers. The water tank was put on a manual swivel stage. So that it was possible to let the ultrasound propagation direction perpendicular to the quartz target, and to get the reflected ultrasound wave with maximum amplitude.

Table 4.1 Operational setting of the Pulse-Receiver equipment.

Parameters	Setting Value
Pulse repetition frequency	1.0 kHz
Input energy	1 $\mu$ J
Voltage	100 V
Damping	50 $\Omega$
Attenuation	0 dB
Gain	20 dB
Low pass filter	15 MHz
High pass filter	500 kHz

#### 4.1.1.2. Results

Figure 4.2 shows the pulse-echo response waveform and power spectra of the PVDF transducer. The transducer has a center frequency about 10.1 MHz and -6 dB bandwidth about 9.2 MHz (range: 5.5 ~ 14.7 MHz, 91.1% fractional bandwidth). Figure 4.3 shows the pulse-echo response waveform and power spectra of the PMN-PZT transducer. The power spectra show that the PMN-PZT transducer has center frequency about 6.2 MHz with a -6 dB bandwidth about 5.6 MHz (range: 3.4 ~ 9.0 MHz, 90.3% fractional bandwidth). Both two transducers have wide fractional bandwidth more than 90%.

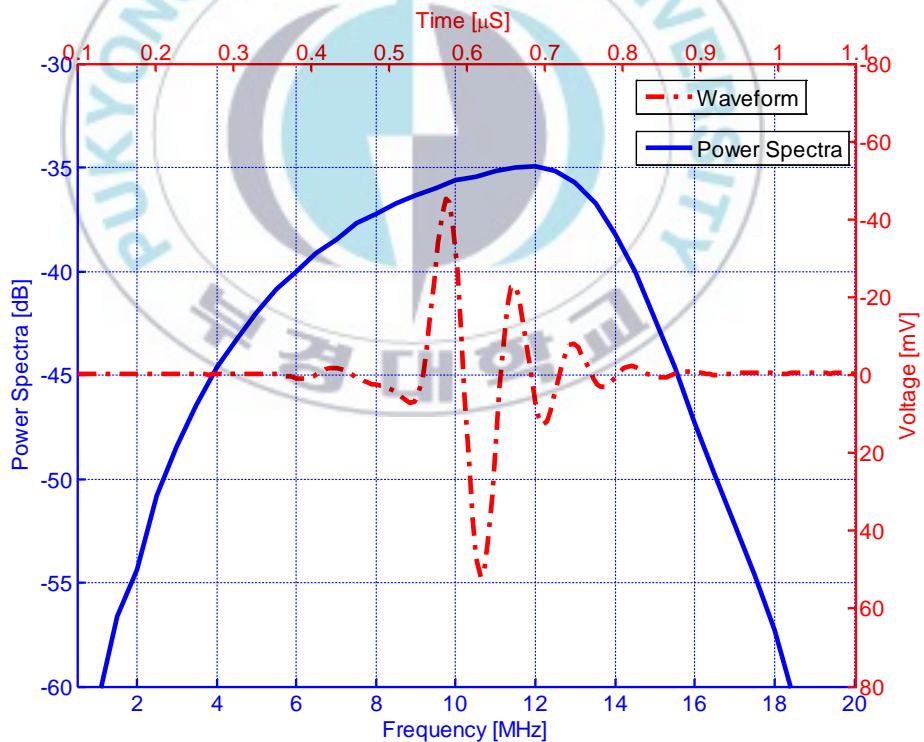


Fig. 4.2 Pulse-echo response characteristics of the PVDF transducers.

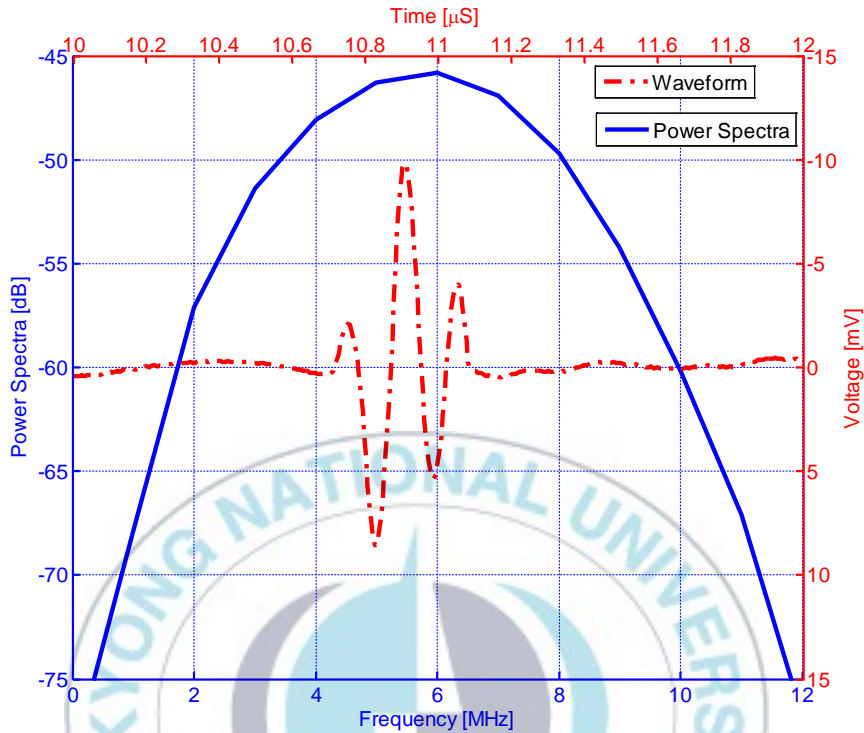


Fig. 4.3 Pulse-echo response characteristics of the PMN-PZT hydrophone.

## 4.1.2. Circular array transducers

As introduced in Section 3.2.2.1, the PVDF circular array transducer was directly fabricated by bonding PVDF film and CCP array pattern on the circle arc acryl backing blocks. So, all elements were tightly fixed. It is difficult to obtain its pulse-echo signal by the method for single element transducer as introduced in Section 4.1.1.1.

### 4.1.2.1. Experiments

Figure 4.4 shows the pulse-echo response measurement system for the circular

array transducers. The transducer was connected with the Pulse-Receiver by a cable with BNC connector. The setting parameters of the Pulse-Receiver were the same as shown in Table 4.1. The quartz target was fixed by an iron stand and inserted into the fluid chamber of the transducer. The transducer was put on a manual swivel stage, which was used to adjust the transducer to be vertical to the quartz target. So that, the reflection wave with maximum amplitude could be received. A Pulse-Receiver equipment (MKCNDT XTR- 2020, MKC Korea) and Oscilloscope (LeCroy LT322, Chestnut Ridge, NY) were used in the experiment. The setting parameters of the Pulse-Receiver and Oscilloscope were the same as the setting in Section 4.1.1.1.

The PMN-PZT circular array transducer was made of 120 independent PMN-PZT hydrophones. So that, the pulse-echo responses could be measured before they were fixed into the plastic base with 120 channels. These hydrophones had the same properties as the one which has been discussed in Section 4.1.1.2.

For measurement of pulse-echo responses of 120 elements of the transducer, a switch circuit was used during the experiment. The switch circuit is shown in Fig. 4.5. It contains a D-sub Screw Terminal Block (National Instruments), a LFH160 Connector (National Instruments) and a Ni PXI-2576 Connector (National Instruments). One side of the switch circuit is connected with the elements of transducer, and the other side is connected with computer which has LabVIEW software. By controlling of LabVIEW, the working elements of the transducer could be easily chosen.

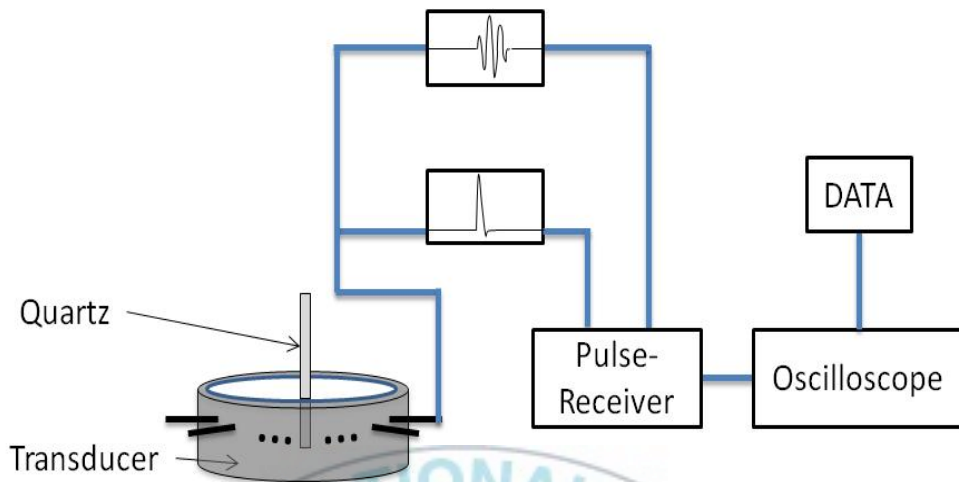


Fig. 4.4 Pulse-echo response measurement system for the PVDF circular array transducer.

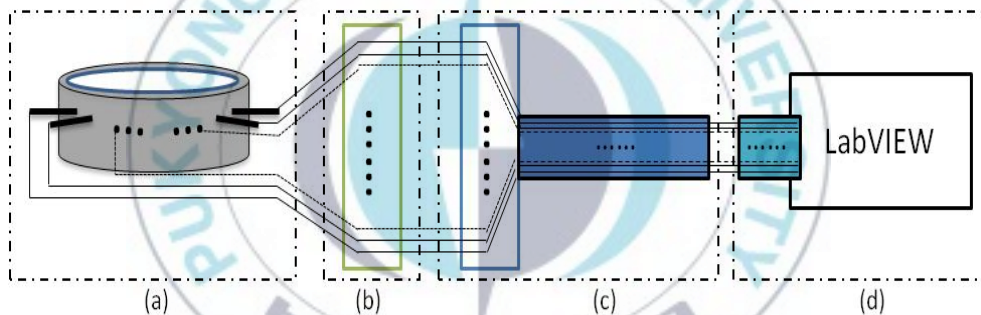


Fig. 4.5 Switch circuit for circuit-array transducer. (a) 120-element circular array transducer, (b) D-sub Screw Terminal Block, (c) LFH160 Connector and (d) Computer with Ni PXI-2576 Connector and LabVIEW software

#### 4.1.2.2. Results

The pulse-echo response of one element of the PVDF array transducer is shown in Fig. 4.6. The power spectra show that the transducer has a center frequency about 11.3 MHz and -6 dB bandwidth about 5.7 MHz (range: 8.5 ~ 14.2 MHz, 50.4% fractional bandwidth).

Comparing with PVDF single element transducer as discussed in Section 4.1.1, it

is found that there is a significant difference of the bandwidth (9.2 MHz bandwidth of single element transducer). And there is also a small change of center frequency. These differences might be due to the different thicknesses of the CCP layers of the two kind transducers. Another reason might be the different thicknesses of bonding epoxy (EPO-TEK 301) between all layers. It is easy to control the pressure evenly during the bonding process for a plane surface transducer than a curved one.

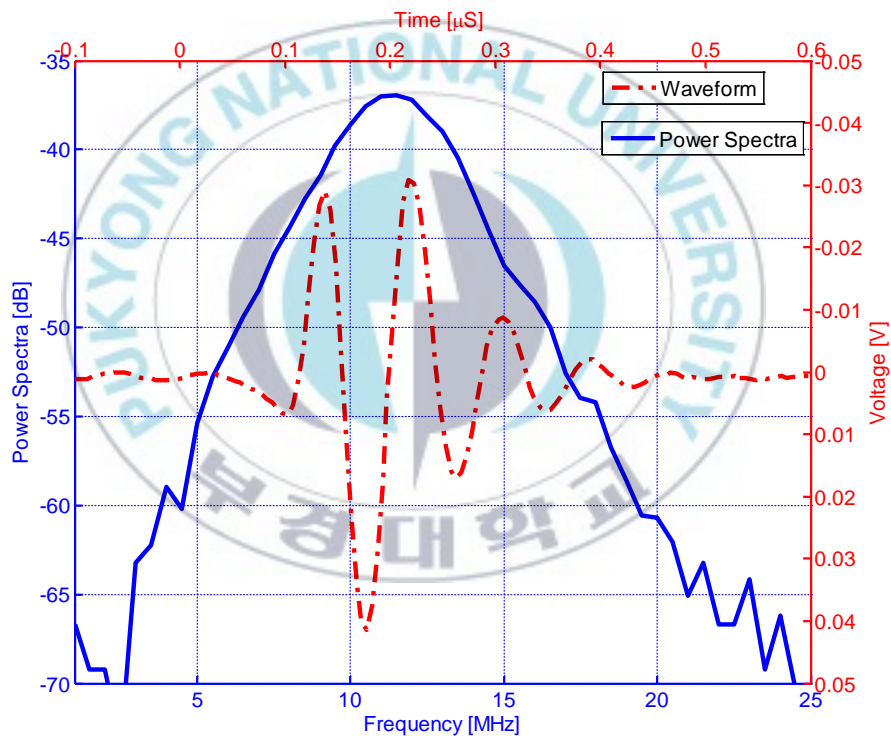


Fig. 4.6 Pulse-echo response characteristics of the PVDF annular-array transducer.

For the other circular array transducer, it was made by 120 single element PMN-PZT hydrophones. Its pulse-echo response signal is the same as the one of the

single element shown in Fig. 4.4.

## 4.2. Receiving sensitivity

In PA imaging system, the transducers or hydrophones just act as detectors of ultrasound signals. Their ultrasound receiving sensitivities affect the final PA images. In this section, the transducers and hydrophones are used to detect the ultrasound waves which are generated by an ultrasound transducer for NDT. The receiving sensitivities of the fabricated single element transducers and circular array transducers are measured using a 5 MHz transducer as a source.

### 4.2.1. Single element transducers

#### 4.2.1.1. Experiments

Figure 4.7 shows the experimental setup of receiving sensitivity measurement of the fabricated single element transducers. As shown in Fig. 4.7, a 5 MHz transducer (A332S, Olympus NDT) was used as the source of sound wave. It was operated by an impulsive signal with  $V_{\text{peak}} = 100 \text{ V}$ , which was offered by Pulser-Receiver equipment (MKCNDT XTR- 2020, MKC Korea).

The generated sound wave propagated in water. Then it was detected by the fabricated transducers which were perpendicular to the surface of the 5 MHz source transducer. By using a pre-amplifier (HP 8447D Amplifier), the received signals were amplified by 25 dB. After that, the signals were shown in an oscilloscope (LeCroy LT322, Chestnut Ridge, NY) and saved by a personal computer (PC). Table 4.2 shows the setting parameters of the Pulser-Receiver equipment and Pre-Amplifier.

In addition, the sound signal was measured by a commercial High Performance PVDF Hydrophone ( $\Phi = 0.2 \text{ mm}$ , 10 kHz ~ 60 MHz, Precision Acoustic Ltd) with an 8 dB DC coupler. And this obtained signal acted as a reference signal in this study.

Table 4.2 Operational setting of the Pulse-Receiver and Pre-Amplifier.

Equipment	Parameter	Setting Value
Pulser-Receiver	Pulse repetition frequency	1.0 kHz
	Pulse width	100 nS
	Voltage	100 V
Pre-Amplifier	Gain	25 dB

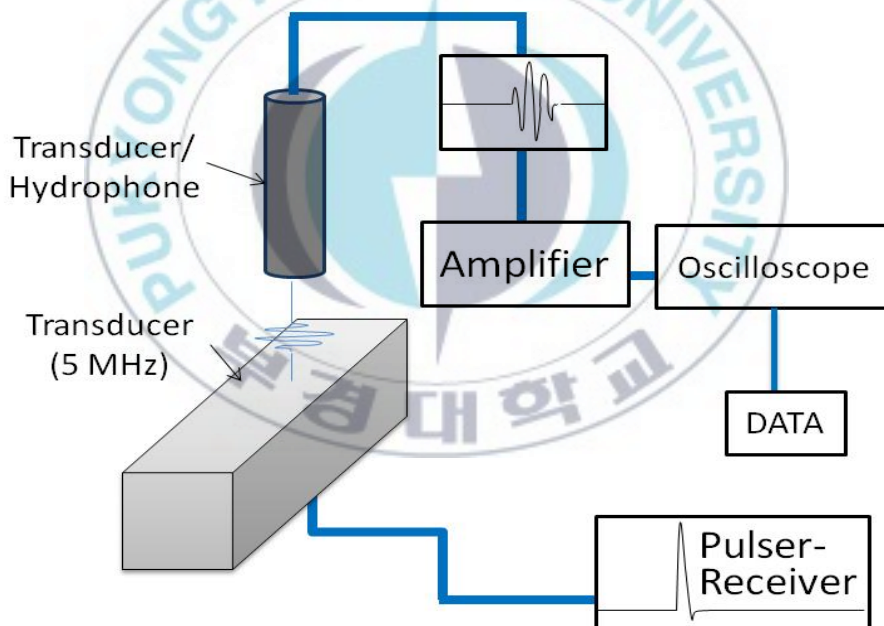


Fig. 4.7 Experiment setup of the ultrasound response measurement.

#### 4.2.1.2. Results

Figure 4.8 shows the received signals by the PVDF and PMN-PZT single element transducers. Both two transducers obtained the similar waveforms of the sound

signals. The receiving sensitivity of the PMN-PZT transducer ( $V_{pp} \approx 90$  mV) is higher than that of the PVDF transducer ( $V_{pp} \approx 50$  mV). However, the signal received by PVDF transducer has ringing with lower level than the PMN-PZT transducer. By comparing with the reference signal as shown in the insertion in Fig. 4.8, the waveforms received by two fabricated transducers are a little bit different for the reference signal.

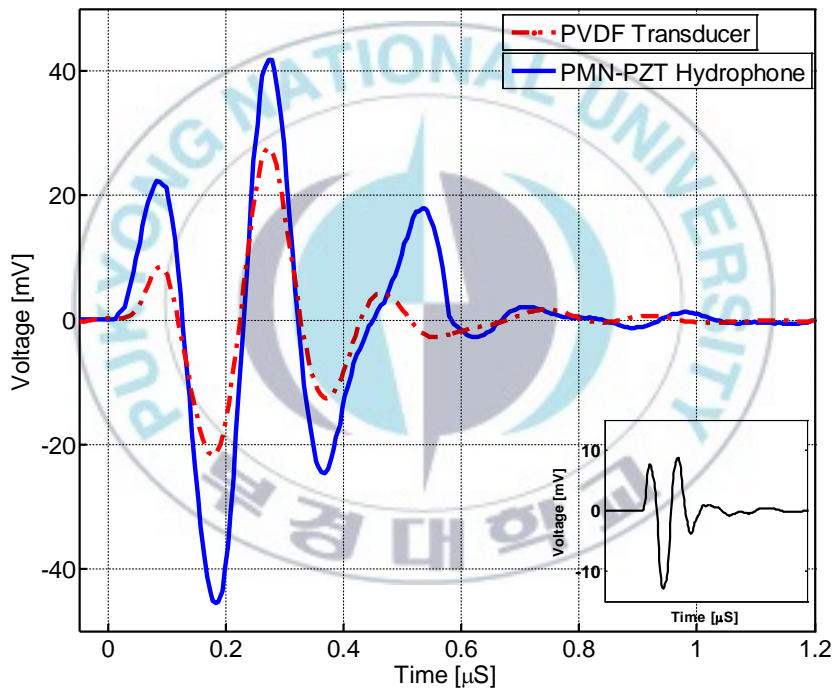


Fig. 4.8 Ultrasound signals received by the PVDF and PMN-PZT transducers. (Insertion is the ultrasound signal received by a commercial High Performance PVDF Hydrophone.)

## 4.2.2. Circular array transducers

### 4.2.2.1. Experiments

Instead of the 5 MHz NDT transducer, a cylindrical PZT transducer was used as the source in this experiment. As shown in Fig. 4.9, the PZT source transducer (4.5 MHz center frequency) was set in the center of the water chamber of the PVDF array transducer. It was excited by an impulsive signal with  $V_{\text{peak}} = 100$  V. The generated ultrasound signals were detected by the elements of PVDF circular array transducer, respectively.

For PMN-PZT circular array transducer, all 120 elements are moveable. It is possible to measure their receiving sensitivity before making the array transducer. So, the setup of the measurement is the same as the one used in Section 4.2.1.1.

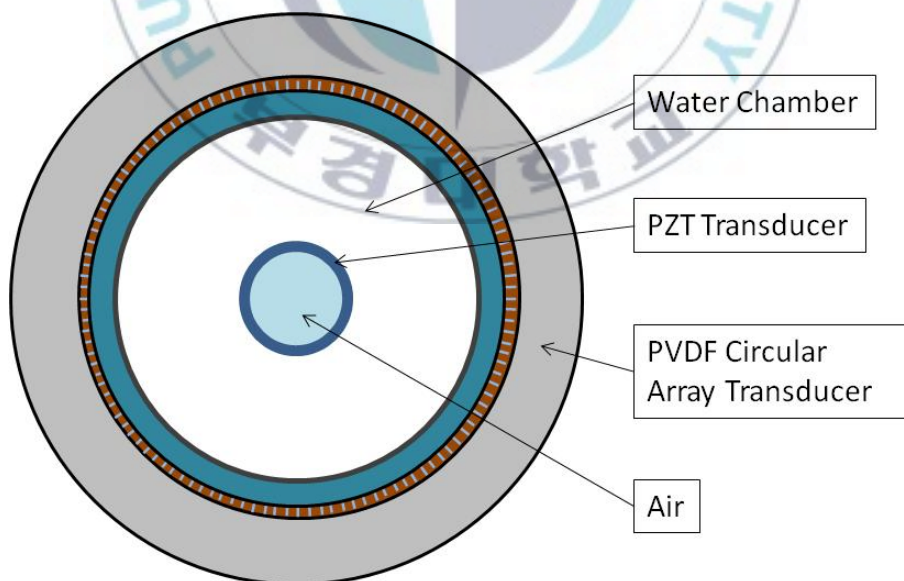


Fig. 4.9 Schematic diagram of a PZT transducer (sound source) and the PVDF array transducer.

#### 4.2.2.2. Results

Because the new PZT transducer was used as sound source for receiving sensitivity measurement, the sensitivity of the PVDF array transducer could not compare with other fabricated transducers. Only the sensitivities of 120 elements of the transducer were compared in this study. Figure 4.10 shows the variation of relative sensitivity ( $V_o/V_i$ ) for 120 elements. It shows the significant differences between the elements. The sensitivity deviation of the transducer is in a range from -47.1 dB to -37.9 dB.

Figure 4.11 shows the variation of the relative sensitivity ( $V_o/V_i$ ) for 120 elements of the PMN-PZT circular array transducer. It is found that the variation of the sensitivity is much smaller than that shown in Fig. 4.10. The average sensitivity is about -40.1 dB and the sensitivity deviation is less than  $\pm 1.5$  dB.

By comparing the sensitivity variations of two array transducers, the PMN-PZT transducer shows much high uniformity than PVDF transducer. The poor uniformity of PVDF transducer may due to the thickness changing of the epoxy bonding layers between PVDF film, CCP layer and acryl backing block. Two thick epoxy layers could decrease the center frequency and sensitivity.

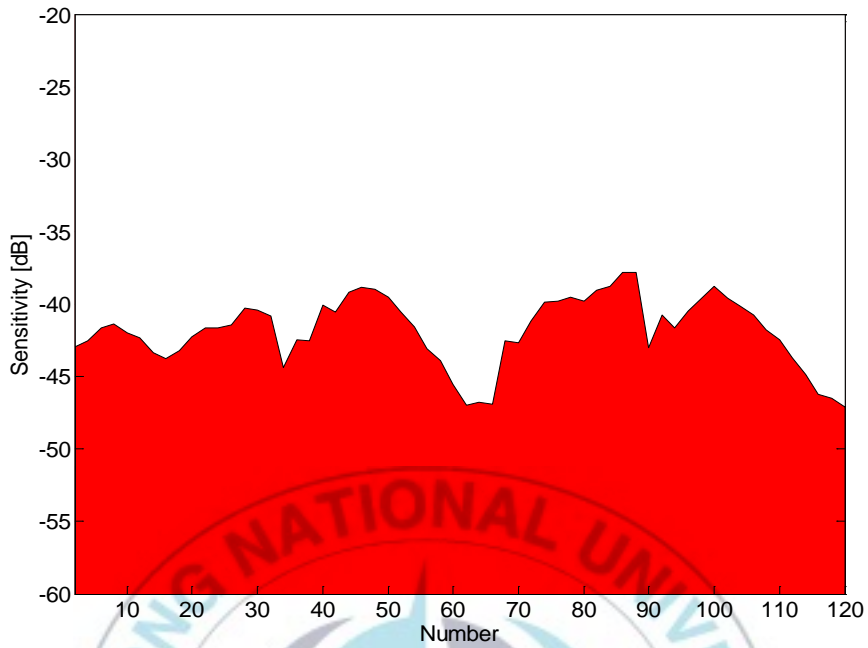


Fig. 4.10 Variation of sensitivity of 120 elements of the PVDF circular array transducer.

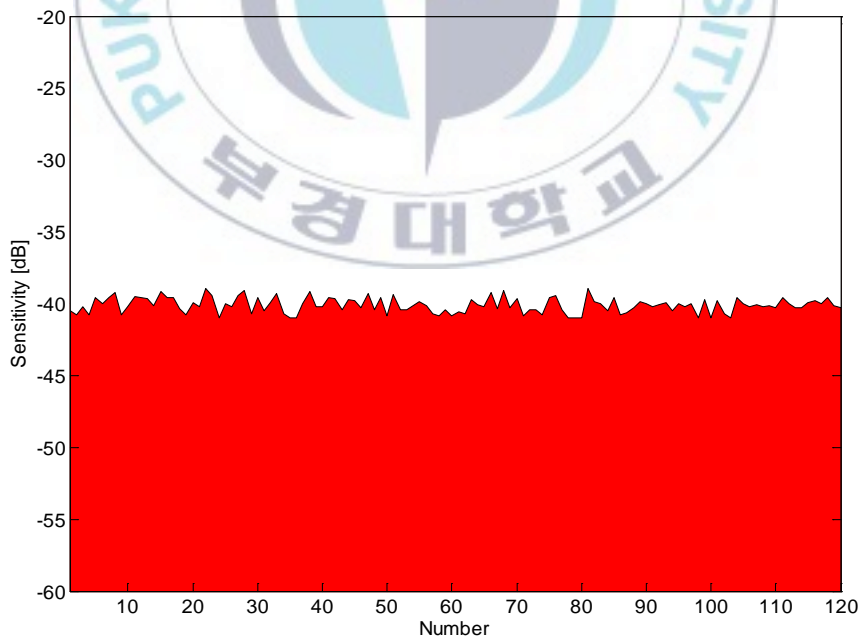


Fig. 4.11 Variation of sensitivity of 120 elements of the PMN-PZT circular array transducer.

### 4.3. Summary

The pulse-echo response and receiving sensitivity of the fabricated transducers were measured and compared. The PMN-PZT and PVDF single element transducers have wider bandwidth ( $> 90\%$  fractional bandwidth). The PMN-PZT transducer has a high receiving sensitivity than PVDF transducer. If the sizes of them are considered, the PMN-PZT transducer is a better choice for making circular array transducer.

The PMN-PZT circular array transducer has a wider bandwidth ( $> 90\%$  fractional bandwidth) than PVDF circular array transducer ( $50.4\%$  fractional bandwidth). The PMN-PZT array transducer has good uniformity. But the uniformity of the PVDF array transducer is so poor that it is impossible to apply to PA imaging system.

According to the characteristics comparison of the fabricated transducers, the PVDF and PMN-PZT single element transducers and PMN-PZT circular array transducer will be applied to PA imaging systems in the next chapter.

## 5. PA imaging

According to the characteristics shown in Chapter 4, three fabricated transducers were applied for PA imaging. They were two single element transducers and one circular array transducer.

For different kinds of transducers, the PA imaging methods are different. PA imaging system based on scanning acoustic microscopy approach will be used for two single elements transducers. Another system based on tomography approach will be used for the circular array transducer.

### 5.1. Scanning acoustic microscopy approach

#### 5.1.1. Imaging system

Single element transducers are mostly used for PA imaging. For this kind of transducers, scanning acoustic microscopy approach is suitable. This kind of imaging approach is widely used in reflection mode PA imaging system which has been successfully applied to *in-vivo* structural, functional, and molecular imaging. Kwang et al.[108] used a deep reflection mode PA imaging system for biological tissue, and successfully obtained the noninvasive PA image of the spleen of a rat. As shown in Fig. 5.1, their PA imaging system contains a 5 MHz central frequency focal transducer which is set in the center of an optical condenser. By controlling of computer, the sample is scanned by this PA imaging system. Wang et al.[109] used another reflection mode system for PA imaging of neonatal brain phantom which contained a piece of newborn infant skull and simulated vessel. A 10 MHz central

frequency transducer was used in this system. The system obtained clear C-scan transcranial PA image of the sample.

If the center frequency of transducer is higher than 30 MHz, this PA imaging system is called PA microscopy (PAM) system. The PAM system could obtained images with high resolution. L. V. Wang et al.[57] have reported their PAM system which is similar to the system as shown in Fig. 5.1. By using high center frequency transducers (50 MHz), the PA imaging with high resolution were obtained (15  $\mu\text{m}$  axial resolution and 45  $\mu\text{m}$  lateral resolution).

Besides the single element transducer, array transducers (such as linear array and annular-array) were also applied to a reflection mode system for PA imaging[69,110].

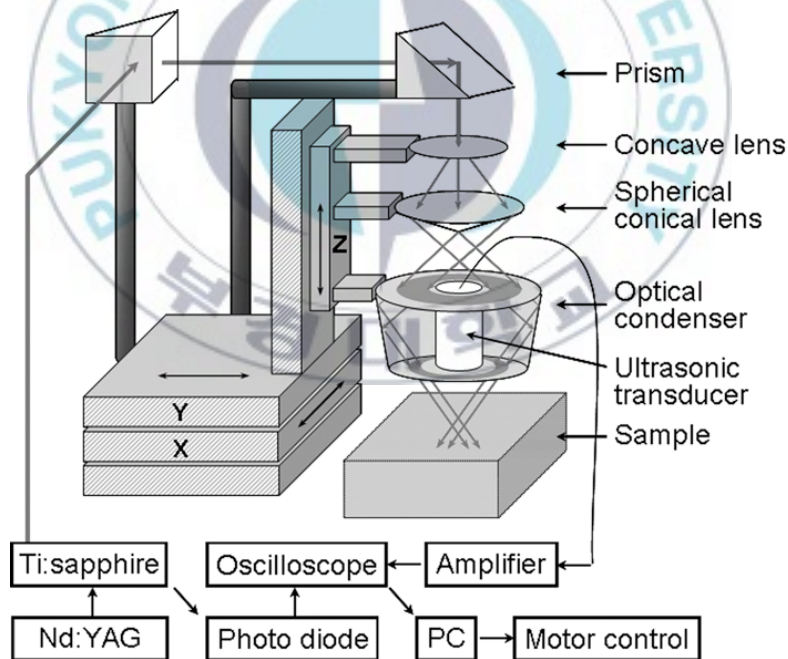


Fig. 5.1 Schematic diagram of the deep reflection-mode photoacoustic imaging system. [57]

### 5.1.2. Experiment

In this study, a kind of PA imaging system based on scanning acoustic microscopy approach was used by single element transducer. Figure 5.2 shows schematic diagram of the system. A Q-switched Nd:YAG laser (Surelite II, Continuum) with 700 nm wavelength pumped by a tunable optical parametric oscillator (Surelite OPO Plus) delivered 5 ns pulses with 10 Hz PRF. The laser was propagated and illuminated the sample by an optical fiber, which was near to the sample. A NIR optical wavelength, 700 nm, was mainly used for PA excitation. The laser pulse was incident on the sample with pulse energy about  $77.2 \text{ mJ/cm}^2$ . Beside the optical fiber, the transducer was set for PA signal detection.

Figure 5.3 shows the setting of the optical fiber, transducer and sample. The sample was a curved silicon pipe ( $\Phi_{inner} \approx 1 \text{ mm}$ ,  $\Phi_{outer} \approx 2 \text{ mm}$ ) which was filled with the solution of Single-Walled Carbon Nanotubes (SWCNTs, 0.1 wt.%). It was set on the horizontal plane by a holding stand. The optical fiber was set near the sample in a slantwise direction. The transducer was perpendicular to the horizontal sample.

When the sample in the water chamber was excited by the laser, the conserved energy generated the PA signal. The PA signal was detected by the transducer. Then it was amplified and stored by a computer.

Finally, the obtained PA signals were transformed to PA images according to reconstruction algorithm process, which was a software package made by computer software (Matlab; MathWorks).

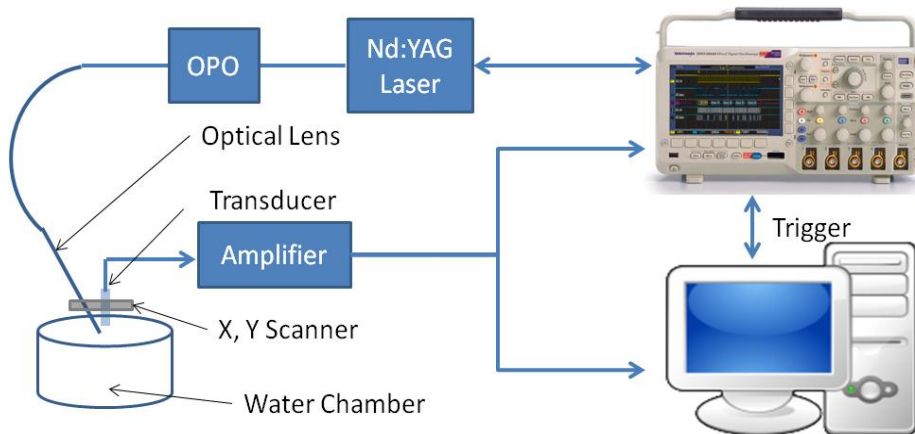


Fig. 5.2 Schematic diagram of the PAM system with single element transducer.

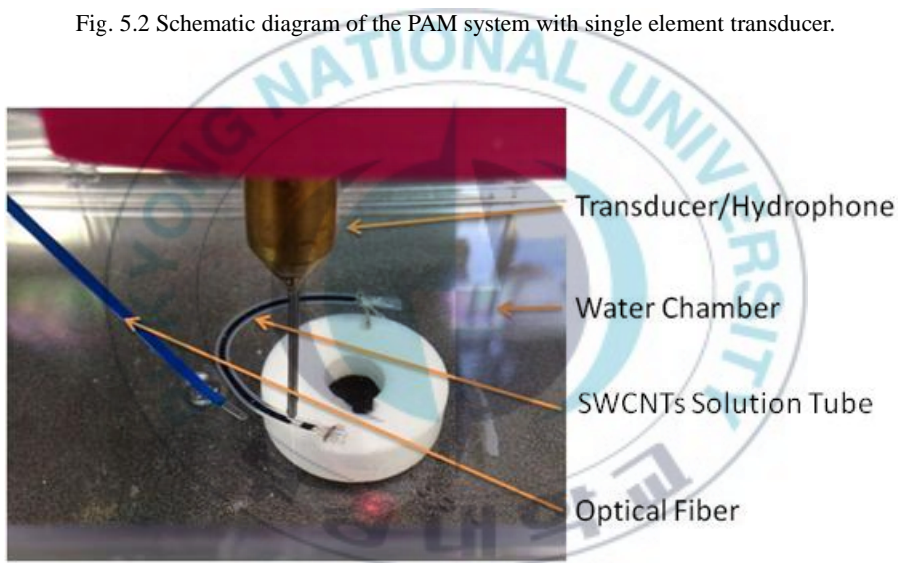


Fig. 5.3 Photograph of the setting details of optical fiber, transducer and SWCNT sample.

## 5.1.3. Results

### 5.1.3.1. Single element transducers

The PVDF and PMN-PZT single element transducers were used in a reflection mode system for PA imaging of the SWCNTs samples, respectively. Figure 5.4 shows

the sample for PA imaging by using the PVDF transducer. The transducer scanned over the sample within the scanning area. Figure 5.5 is the PA image of the sample. The image of the copper wire, which was used to hold the sample, was also obtained by this PA imaging system. However, the quality of the image is not good. The noise level is so high that the contrast of the image is poor.





Fig. 5.4 Sample for PA imaging to use the PVDF transducer.

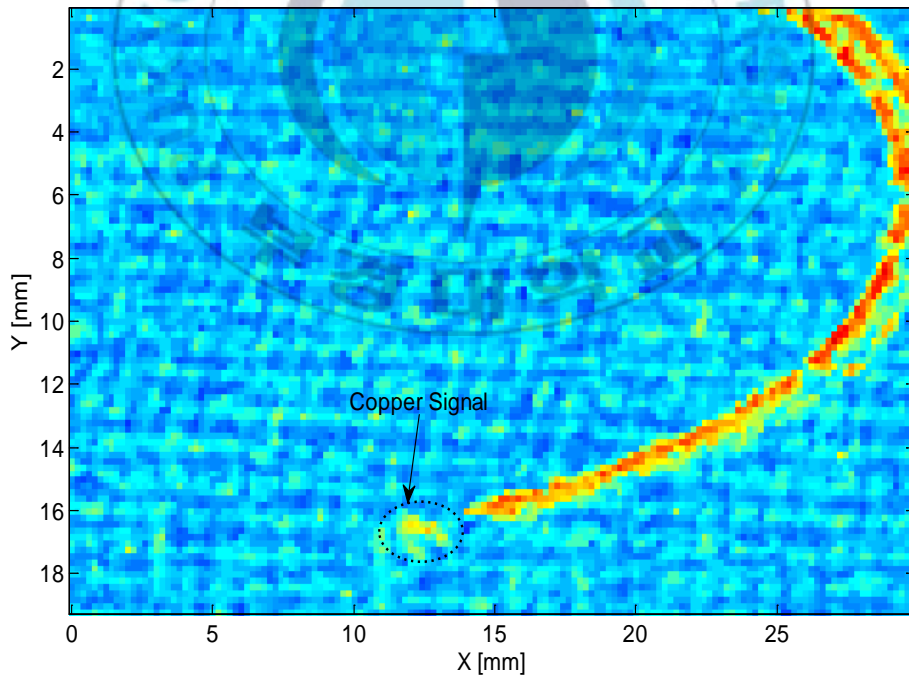


Fig. 5.5 PA image obtained by the PVDF transducer.

Figure 5.6 shows the sample for PA imaging by using the PMN-PZT transducer. The SWCNTs solution and silicon tube of the sample is the same as the one shown in Fig. 5.6. However, the size is smaller than that in Fig. 5.4. The obtained PA image of the sample is shown in Fig. 5.7. It shows the clear shape of the sample. The PA image of copper wire is found and the density difference of the solution could be known. Due to the bubbles in the sample, the obtained image is not completely tube likes.



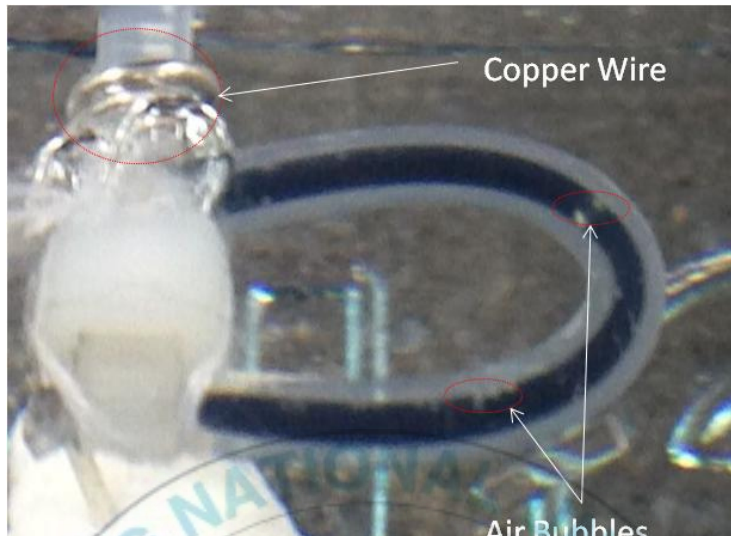


Fig. 5.6 Sample for PA imaging using PMN-PZT transducer.

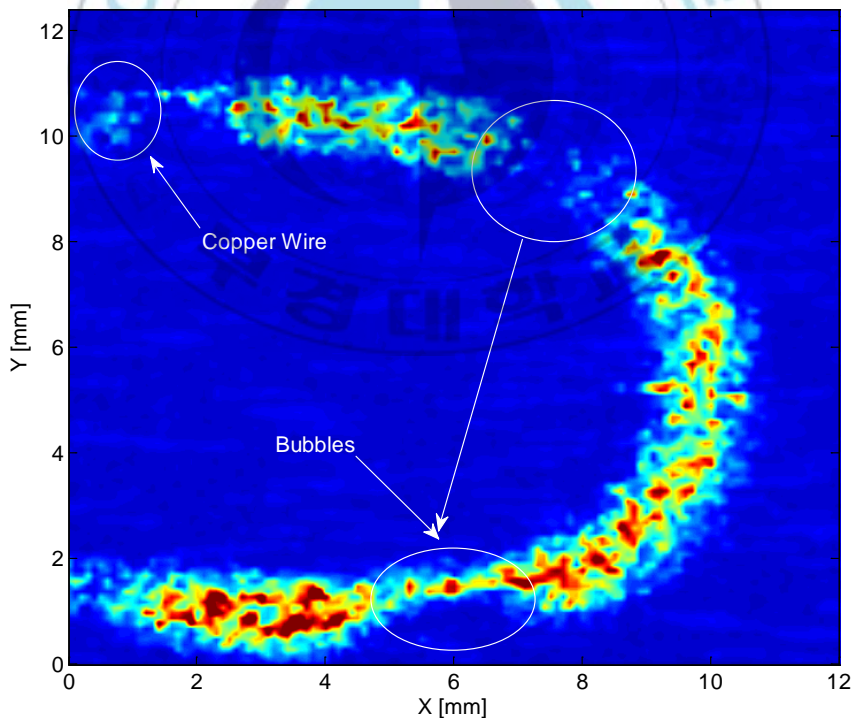


Fig. 5.7 PA images obtained by the PMN-PZT transducer.

Comparing Fig. 5.5 and Fig. 5.7, it is found that the PA image obtained by PMN-PZT transducer has better quality than the one obtained by PVDF hydrophone. The former shows the significantly higher contrast than the other.

### 5.1.3.2. Circular array transducers

Figure 5.8 shows the photograph of sample A and B (two copper wires with  $\Phi_A=1.0$  mm and  $\Phi_B=0.35$  mm) which were set in the chamber of the PMN-PZT circular array transducer for PA imaging. The samples were scanned by the laser. And the PA signals were received by all elements of the array transducer and stored on a computer.

The PA imaging obtained by scanning acoustic microscopy approach using PMN-PZT array transducer is shown in Fig. 5.9. However, the shapes of the samples' images are different from the real samples. It is found from the right insertions that the images of samples A and B are not circular point but irregular lines. This is due to the unsuitable PAM imaging method, which is good at imaging of a 2-D plane by scanning. Another reason might be the setting error of some elements which is a little near or far from the center of the chamber.

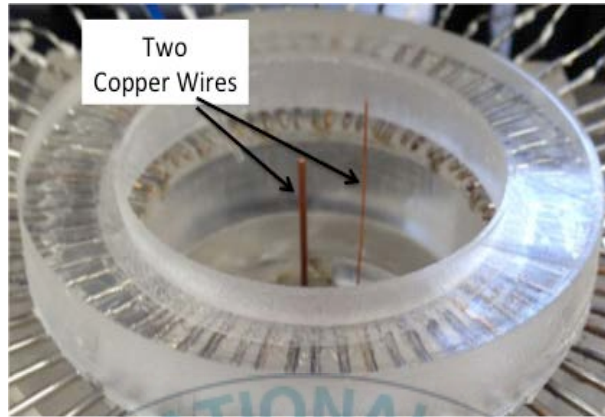


Fig. 5.8 Samples for PA imaging in chamber of the PMN-PZT circular array transducer.

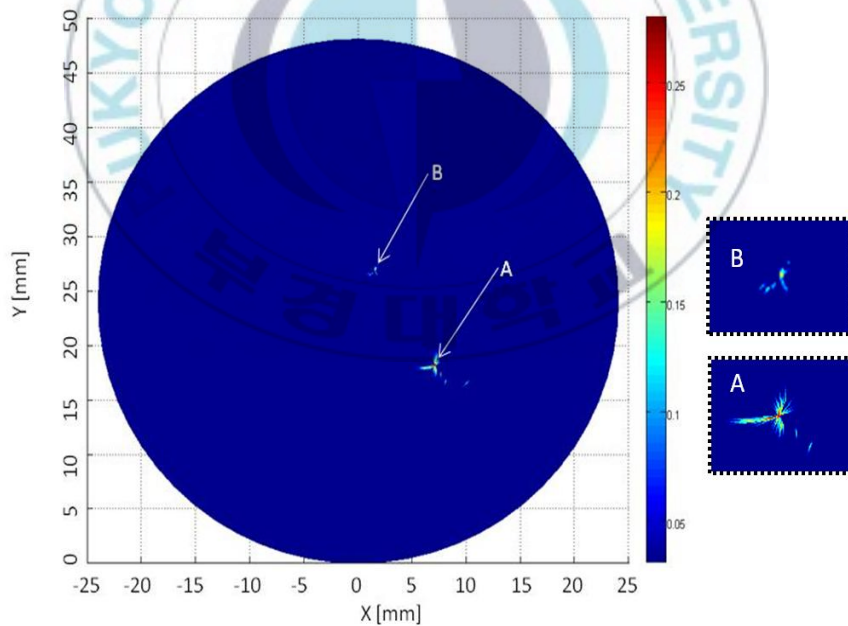


Fig. 5.9 PA image of the sample obtained by scanning acoustic microscopy approach using the PMN-PZT circular array transducer.

## 5.2. Tomography approach

### 5.2.1. Imaging system

PA imaging by tomography approach is also called PAT imaging, which is a hybrid imaging method combining photoacoustic effect and computerized tomography technology. Many reports of the PAT system are using linear array transducers for signal detection. T. Chaigne et al.[111] used a PAT system for PA imaging of leaf skeleton. As shown in Fig. 5.10, the linear array transducer (128 elements 14.4 MHz center frequency, Vermon, France) is used for PA signal detection.

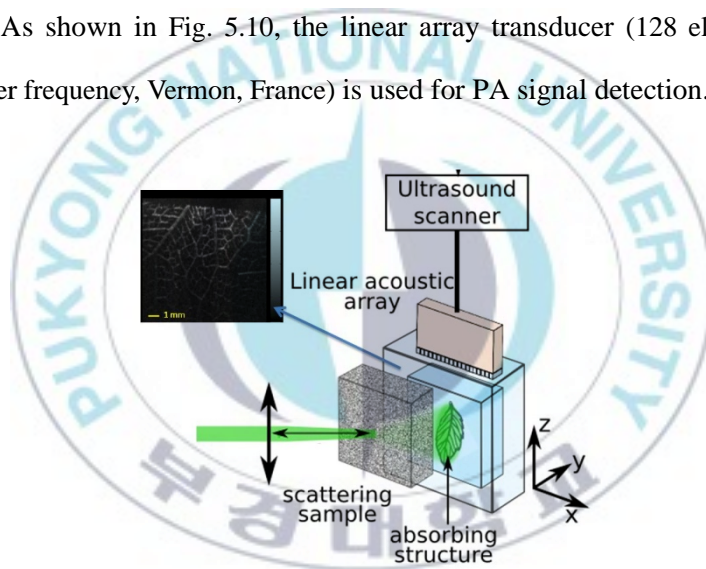


Fig. 5.10 Schematic diagram of a PAT system with linear array transducer. [111]

In the circular-view PAT system, the ultrasound detection follows a ring[36,112]. A pulsed laser beam is expanded to illuminate the object and an ultrasonic transducer scans around the object in a circle to acquire the photoacoustic data. An inverse algorithm converts the photoacoustic data to the initial photoacoustic pressure distribution, which is an image of the cross-section containing the scanned circle.

Although there are many research works focusing on PAT, the works about circular

array transducers for PA imaging using are rarely reported. L. V. Wang's [70,113] research team in Washington University has done a lot of work by using a 1-3-piezocomposite circular array transducer which is fabricated by Imasonic (Besancon, France). The transducer has a 5 MHz central frequency, 80% bandwidth and 512 elements. By this system, the PA image of small animals and leaves are obtained with high resolution about 0.2 mm.

It could be found that the mechanical scanning is necessary when a single element or linear array transducer is used in a PAT imaging system. To obtain a PA image in a short time, it is necessary to design and fabricate a circular array transducer.

### **5.2.2. Experiment**

Figure 5.11 is the schematic diagram of the PA imaging system based on tomography approach (PAT) used in this study. It is different from the system as shown in Section 4.1.2. The samples used in the PAT experiment were the same as the ones shown in Fig. 4.11. The optical fiber was perpendicular to the array transducer and was about 10~12 mm upper of the sample. Due to the laser refraction from laser fiber to water (index of refraction  $n \approx 1.33$ ), the laser beam was expanded to illuminate the sample in a circular shape ( $R = 11.3\sim 13.6$  mm). And the laser delivered the power density about  $35.2 \text{ mJ/cm}^2$ . The setting parameters of the laser were the same as the ones used in Section 4.1.2. The 120-element PMN-PZT circular array transducer was used as the ultrasound detector in the system. The top side of the copper samples was almost at the same height as the hydrophone array. The DAQ circuit in this PAT system was the same as the one introduced in Section 3.1.2.1 and shown in Fig. 3.5.

At last, the obtained data from 120 PMN-PZT hydrophones were used to reconstruct a PA image. And a reconstruction process was made by Matlab in this study. Because of the illumination area of laser beam in the chamber, the diameter of imaging area was  $\Phi \approx 14$  mm.

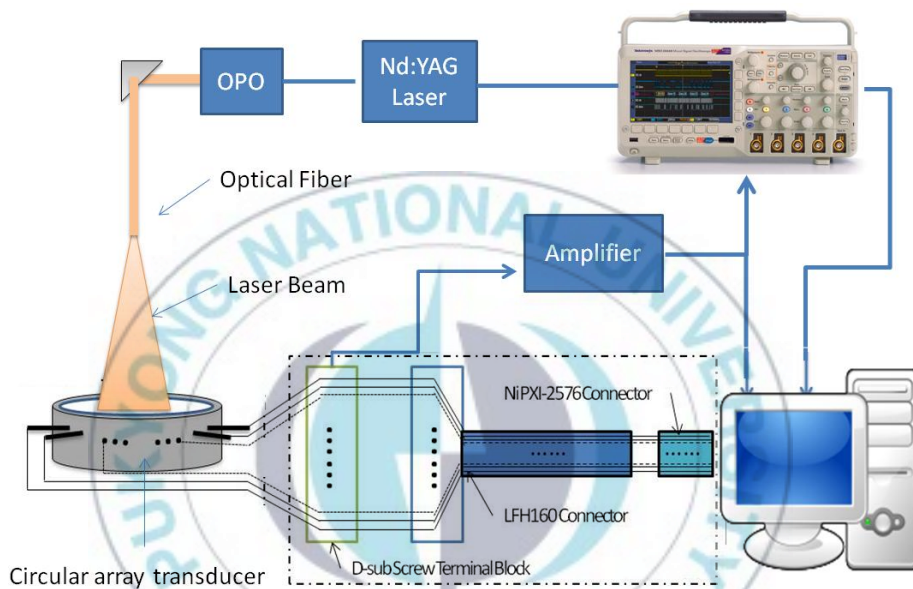


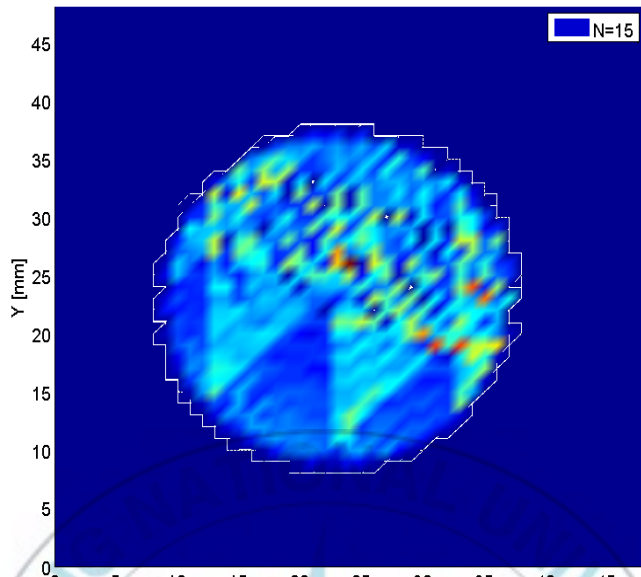
Fig. 5.11 Scheme diagram of the PAT system with the PMN-PZT circular array transducer.

### 5.2.3. Results

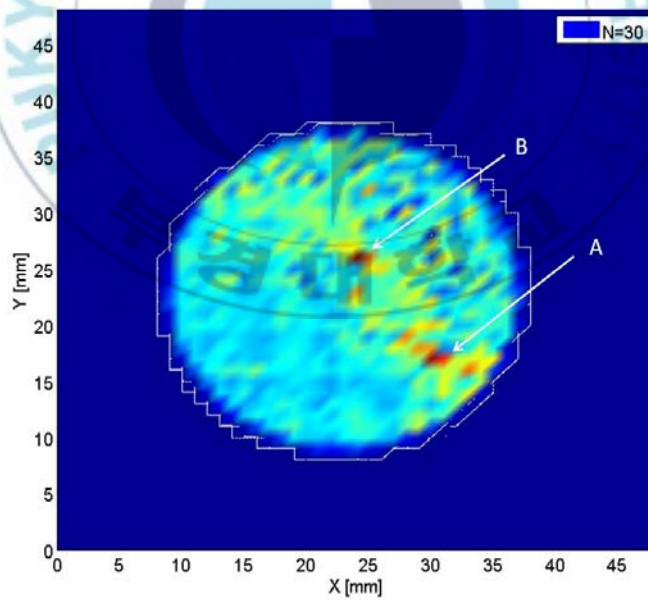
The PMN-PZT circular array transducer was applied to a tomography PA imaging system. The laser beam illuminated the samples simultaneously. The generated PA signals from the samples were detected by the elements of transducer at the same time. By using a back projection reconstruction algorithm in time domain, PA images were formed.

### 5.2.3.1. PA imaging using different number of elements

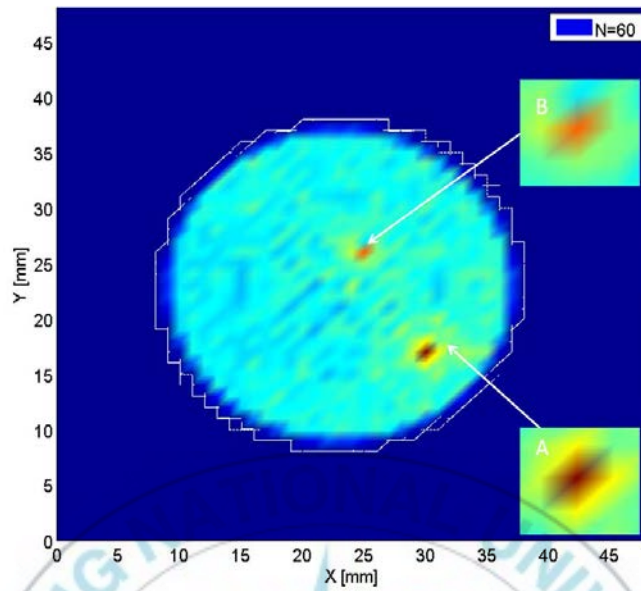
The influence of the number of working elements ( $N$ ) of the circular array transducer was analyzed. The size of image pixel was set about  $1 \times 1 \text{ mm}^2$ . Figure 5.12 shows the images obtained by the circular array transducers with different  $N$  (15, 30, 60 and 120). As shown in Fig. 5.12 (a), it is not easy to confirm the position of the samples when  $N = 15$ . The signal to noise ratio (SNR) is too small to distinguish the PA signals from the image. When  $N$  increases to 30, the image of the sample becomes clearer. The position of the sample is marked with A and B. But it is hard to measure the size of the two points. When  $N = 60$  and 120, it is easy to confirm the position of the sample. As shown in the insertions of Fig. 5.12 (c) and (d), the ultrasound intensity of point A (dark red) is higher than point B (light red). They have the same size (hexagon, area =  $3 \text{ mm}^2$ ) which is different from the real size of the sample ( $d_1 = 1.00 \text{ mm}$  and  $d_2 = 0.35 \text{ mm}$ ). The images for  $N = 60$  and 120 are quite similar.



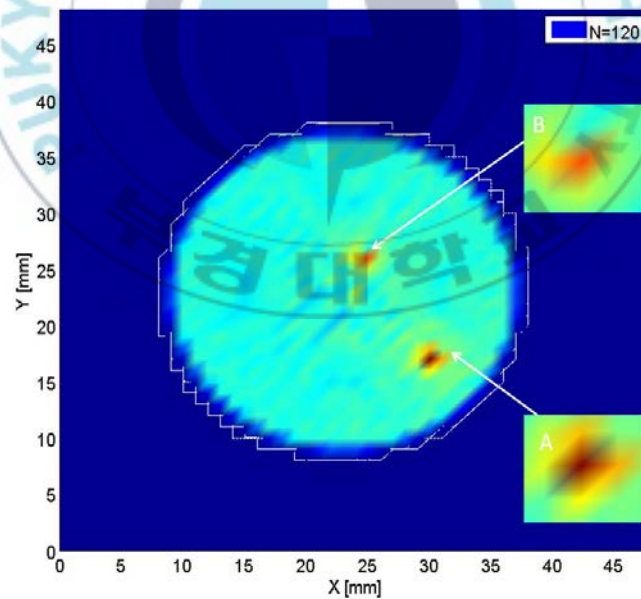
(a)



(b)



(c)



(d)

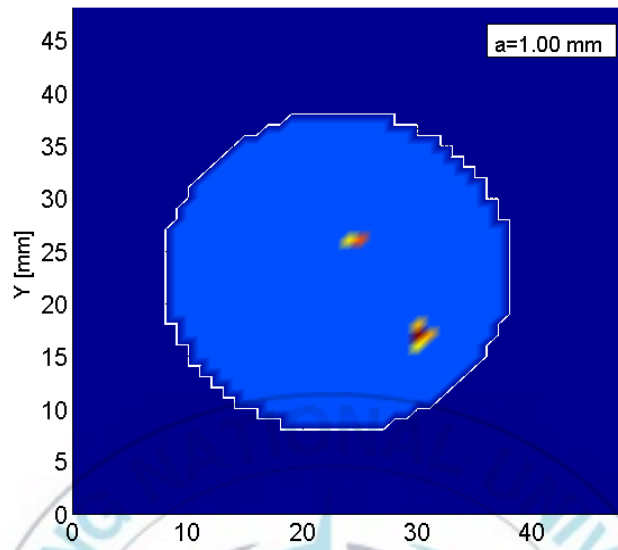
Fig. 5.12 Images of the sample obtained by circular array transducer with different number of working element. (a)  $N=15$ , (b)  $N=30$ , (c)  $N=60$  and (d)  $N=120$

### 5.2.3.2. PA imaging using different size of pixel

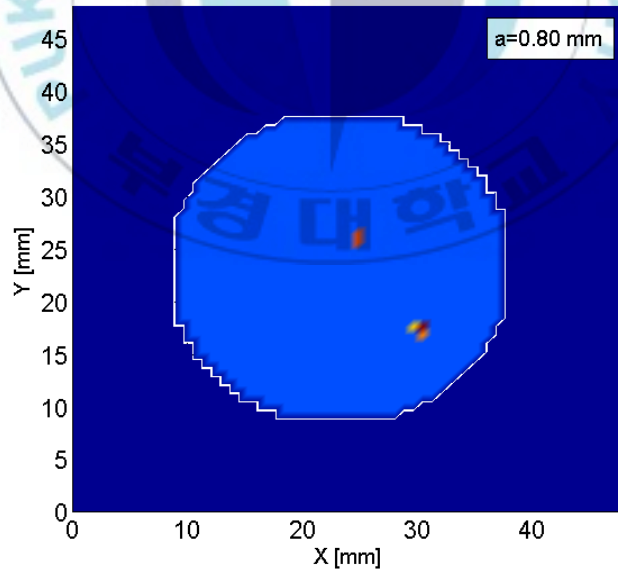
The influence of the pixel size, which was set in the reconstruction process, was analyzed. The pixel is a square at the fixed position of the imaging area. It contains the sound signals at certain position from each element. The data obtained by 120 elements are used to reconstruct the PA image with different setting of pixel size. When the side-lengths 'a' of pixel are 1.0, 0.8, 0.6, 0.4, 0.2, and 0.1 mm, the obtained PA images are shown in Fig. 5.13. According to Fig. 5.13 (a), (b), (c) and (d), the size of image decreases when the pixel size changes from 1.0 to 0.4 mm. From Fig. 5.13 (d), (e) and (f), it is found that the image distorts with the decrease of the pixel size. When  $a = 0.1$  mm, it is impossible to find the samples from the image.

The image of sample is approximated as a circle in all figures. Table 5.1 shows how the diameters of samples in the images change with the increase of pixel size. When pixel size is 0.4 or 0.6 mm, the image size of sample A is close to its real size ( $\Phi \approx 1.00$  mm). But for sample B, the image size is about three times larger than the real size ( $\Phi \approx 0.35$  mm). This is due to the resolution limitation of the transducer.

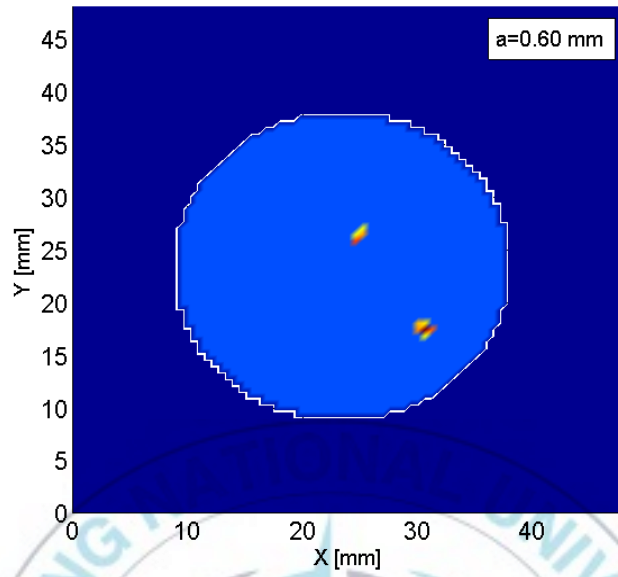
To obtain a PA image with high quality, the pixel size should be near to the resolution of the transducer. Figure 5.14 shows the PA image of the sample when pixel size is set about 0.5 mm. At this time, the image sizes of sample A and B are 1.0 and 0.8 mm which are close to the real size of the samples.



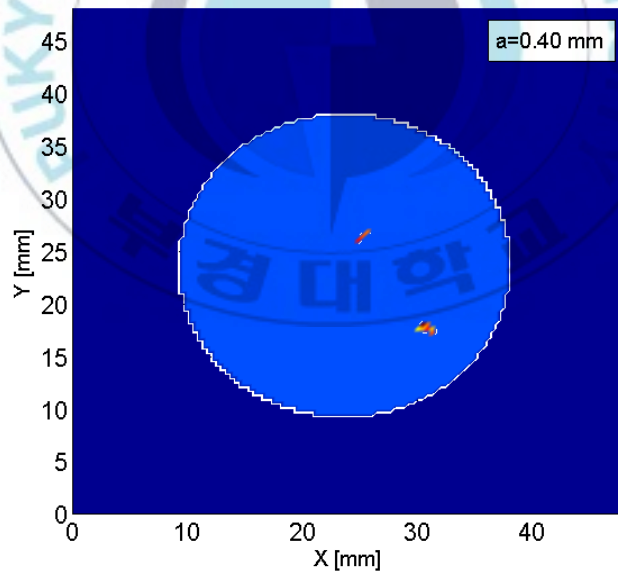
(a)



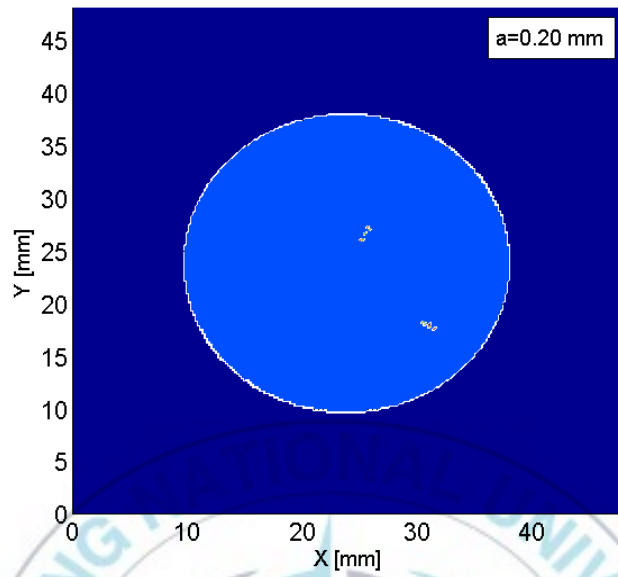
(b)



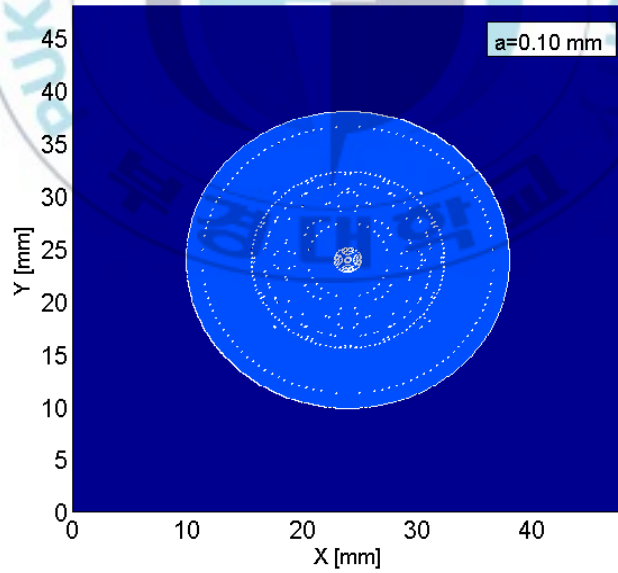
(c)



(d)



(e)



(f)

Fig. 5.13 Images of the sample obtained by the array transducer with different setting size of pixel.

(a)  $a=1.0$  mm, (b)  $a=0.8$  mm, (c)  $a=0.60$  mm, (d)  $a=0.4$  mm, (e)  $a=0.2$  mm and (f)  $a=0.10$  mm.

Table 5.1 Image size of sample changing with the pixel size.

Fig. 4.16	Pixel Size [mm]	Image Size [mm]	
		A	B
(a)	1.0	3.0	2.0
(b)	0.8	2.0	1.5
(c)	0.6	2.0	1.3
(d)	0.4	1.5	1.0
(e)	0.2	-	-
(f)	0.1	-	-

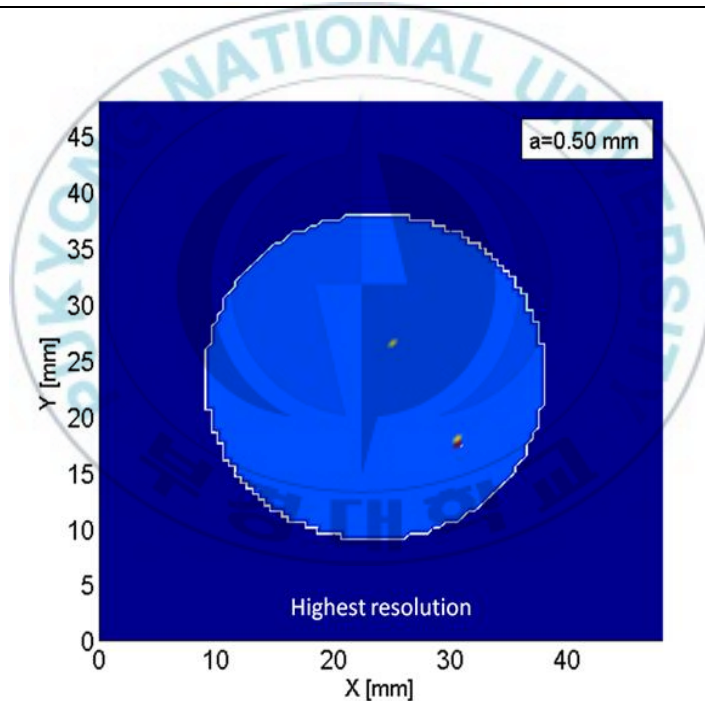


Fig. 5.14 Images of the sample obtained by circular array transducer when pixel size is 0.5 mm.

### 5.3. Summary

In this chapter, the fabricated transducers were applied to PA imaging systems and the obtained PA images were compared. The PVDF and PMN-PZT single element

transducers were applied to a PA imaging system based on scanning acoustic microscopy approach. Both two transducers obtained the images of the SWCNTs samples. The image obtained by the PMN-PZT transducer shows high quality image than that obtained by the PVDF transducer. The latter was affected by noise more than the former. The PMN-PZT array transducer was also applied in this PA imaging system. The samples in the chamber of the array transducer were scanned by laser. The PA image was reconstructed by combining the signals received by all 120 elements. The shapes of the samples shown in the image were very different from the real samples. This PA imaging system was not suitable for the circular array transducer.

Another PA imaging system which was based on tomography approach was used for imaging of the sample in chamber of the PMN-PZT array transducer. An expanded laser beam illuminated an area in which the samples were set. All elements received the PA signals from different sample at the same time. By a tomography reconstruction process, the PA images were successfully obtained. By using the array transducer in this imaging system, the quality of the image was easily affected by number of working elements during measurement and size of pixel during reconstruction.

## 6. Conclusions and future works

### 6.1. Conclusions

#### 6.1.1. Characteristics of transducers

In this study, two piezoelectric materials (28  $\mu\text{m}$  thick PVDF and 310  $\mu\text{m}$  thick PMN-PZT) were used to make to single element (plane surface) and 120 elements circular array transducers.

The characteristics of the fabricated transducers were measured and compared. The PVDF single element transducer has the center frequency about 10.1 MHz. The PMN-PZT single element transducer has the center frequency about 6.2 MHz. Two transducers have similar wide -6 dB fractional bandwidths about 90%. The PMN-PZT shows a higher receiving sensitivity ( $V_{pp} = 90$  mV) than the PVDF transducer ( $V_{pp} = 50$  mV).

The center frequency and -6 dB bandwidth of PMN-PZT array transducer are the same as the PMN-PZT single element transducer. The variation of the receiving sensitivity is in a range about  $\pm 1.5$  dB, which means the uniformity of the transducer is good. The PVDF array transducer has poor uniformity of the relative receiving sensitivity, which varies from -47.1 dB to -37.9 dB. The large variation of the sensitivity is due to the uneven bonding layers (epoxy) between the PVDF film, CCP layer and backing block.

The PMN-PZT single element and circular array transducers and PVDF single element transducer were selected for PA imaging.

### **6.1.2. PA imaging**

Two single element transducers (PMN-PZT and PVDF) were applied in a PA imaging system based on scanning acoustic microscopy approach. A sample for the imaging was SWCNTs solution in silicon tube. Both two transducers could obtain the images of the sample. The poor contrast of the PA image was caused by high noise level of the PVDF transducer. The image obtained by PMN-PZT transducer shows better quality than the other one.

The PMN-PZT circular array transducer was applied in a tomography approach PA imaging system. Two different size copper wires were set in the chamber of the transducer as samples. The results show that the addition of working elements could increase the contrast of PA image. In this study, the best image could be obtained when the number of working elements was more than 60. Besides that, the setting pixel size affected the quality of PA imaging during the reconstruction process. For the fabricated PMN-PZT array transducer, 0.5 mm was the best pixel size for reconstruction of PA imaging. By using the PMN-PZT array transducer, it was possible to obtain PA images with similar size as the samples.

Generally speaking, the PMN-PZT piezoelectric single crystal is a good material for making small transducer (like a hydrophone) with high receiving sensitivity. The PMN-PZT single element transducer and circular array transducer could be applied in PA imaging systems for high quality images.

### **6.2. Future works**

According to this study, we have found that the PMN-PZT transducer could obtain

high quality PA images. The PMN-PZT circular array transducer could be applied for PA image with resolution about 0.5 mm. So, we will try to use this transducer to obtain an image of some biological tissue with size about 0.5 mm.

For PA tomography (PAT) application, it is necessary to fabricate the transducer with high sensitivity, high center frequency and wide bandwidth. And also, the image reconstruction algorithm should be improved for PAT.



## Acknowledgement

Foremost, I would like to express my sincere gratitude to my advisor Prof. Kang-Lyeol Ha, for his continuous support of my Ph.D study and research, for his patience, encouragement and immense knowledge. His guidance has helped me a lot during the last five years of research and living in South Korea.

I would like to thank to Prof. Moo-Joon Kim, Prof. Jong-Rak Yoon, Prof. Hyunwook Kang, Prof. Jung-soon Kim and Prof. Jung-Hwan Oh, for their kindness help in my research. Here, please allow me to give my thanks to some Chinese professors. They are Prof. Yan-Lin Huang from Soochow University who gave me advices and helped me a lot during the past seven years, Prof. Xi-Peng Pu, Prof. Xin-Ming Zhang, Prof. Hai Guo, Prof. Rui-Jin Yu, Prof. Laishun Qin, Prof. Ling Li and Prof. Xiaoguang Liu.

Thanks to all members of 'Well-Bing' tennis club, professors, teachers, uncles and sisters. It is really a great honor to play tennis with them in the past three years. They will be the ones I know I will never forget. Thanks to my Korean friends Jeong-Won Yang, Kwang-Yoon Choi, Mi-Sun Jo, Hui-Uk Lee, Hae-Rang Huang, Yea-jun Park, Ji-Hee Jung, and so on, for their selfless help. Thanks to my Chinese friends Liang Shi, Xue-Bin Qiao, Ming-Ming Zhang, Guo Qiao, Dong-Lei Wei, Ze-Han Jiang, Pei-qing Cai, Shang-Long Zhu, Shi-Wei Liu, Fei Tian, Xiao-Feng Fan, Wen-Yan Wang, Cheng-Xiang Zhan, and so on, for the happy time with you.

At last, I'd like to dedicate this work to my parents. Whatever I do, wherever I go, they will always give me encouragement and strength. And thanks to all my relatives for their endless care and support.

## References

- [1] Karen Kinkel, Ying Lu, Marcus Both, Robert S. Warren and Ruedi F. Thoeni. 'Detection of Hepatic Metastases from Cancers of the Gastrointestinal Tract by Using Noninvasive Imaging Methods (US, CT, MR Imaging, PET): A Meta-Analysis.' *Radiology*, 2002, **224**, p.748-756.
- [2] Maria Raquel Oliva and Sanjay Saini. 'Liver cancer imaging: role of CT, MRI, US and PET.' *Cancer Imaging*, 2004, **4**, p.S42-S46.
- [3] Bell Alexander Graham. 'On the Production and Reproduction of Speech by Light.' *Am J Sci*, 1880, **20**, p.305-324.
- [4] Minghua Xu. 'Photoacoustic computed tomography in biological tissues: algorithms and breast imaging.' DOCTOR OF PHILOSOPHY, Texas A&M University, 2004.
- [5] N. T. Wells P. 'Ultrasonic imaging of the human body.' *Rep Prog Phys*, 1999, **62**, p.671-722.
- [6] B. T. Cox and P. C. Beard. 'Fast calculation of pulsed photoacoustic fields in fluids using k-space methods.' *The Journal of the Acoustical Society of America*, 2005, **117**, p.3616-3627.
- [7] Jerry L. Prince and Jonathan M. Links. 'Medical Imaging Signals and Systems.' Published by *Prentice Hall*, 2014.
- [8] Lihong V. Wang. 'Ultrasound-Mediated Biophotonic Imaging: A Review of Acousto-Optical Tomography and Photo-Acoustic Tomography.' *Dis Markers*, 2004, **19**, p.123-138.
- [9] Zhen Yuan and Huabei Jiang. 'Three-dimensional finite-element-based photoacoustic tomography: Reconstruction algorithm and simulations.' *Med Phys*, 2007, **34**, p.538-546.
- [10] Paltauf and R. Nuster G. 'Experimental evaluation of reconstruction algorithms for limited view photoacoustic tomography with line detectors.' *Inverse Probl*, 2007, **23**, p.S81-S94.
- [11] A. Anastasio and Jin La Mark. 'Application of inverse source concepts to photoacoustic tomography.' *Inverse Probl*, 2007, **23**, p.S2-S35.
- [12] Kornel P. Köstli and Paul C. Beard. 'Two-dimensional photoacoustic imaging by use of Fourier-transform image reconstruction and a detector with an anisotropic response.' *Appl Optics*, 2003, **42**, p.1899-1908.
- [13] Zhen Yuan, Qiang Wang and Huabei Jiang. 'Reconstruction of optical absorption coefficient maps of heterogeneous media by photoacoustic tomography coupled with diffusion equation based regularized Newton method.' *Opt Express*, 2007, **15**, p.18076-18081.

- [14] Roy G. M. Kolkman, Erwin Hondebrink, W. Steenbergen and F. F. M. de Mul. 'In vivo photoacoustic imaging of blood vessels using an extreme-narrow aperture sensor.' *Ieee J Sel Top Quant*, 2003, **9**, p.343-346.
- [15] Christopher P. Favazza, Omar Jassim, Lynn A. Cornelius and Lihong V. Wang. 'In vivo photoacoustic microscopy of human cutaneous microvasculature and a nevus.' *J Biomed Opt*, 2011, **16**, p.16015.
- [16] Roger J. Zemp, Rachel Bitton, Meng-Lin Li, K. Kirk Shung, George Stoica and Lihong V. Wang. 'Photoacoustic imaging of the microvasculature with a high-frequency ultrasound array transducer.' *J Biomed Opt*, 2007, **12**, p.10501.
- [17] Changhui Li, Andres Aguirre, John Gamelin, Anastasios Maurudis, Quing Zhu and Lihong V. Wang. 'Real-time photoacoustic tomography of cortical hemodynamics in small animals.' *J Biomed Opt*, 2010, **15**, p.10509.
- [18] Robert A. Kruger, Pingyu Liu, Yuncai Richard Fang and C. Robert Appledorn. 'Photoacoustic ultrasound (PAUS)—Reconstruction tomography.' *Med Phys*, 1995, **22**, p.1605-1609.
- [19] RY Fang, RA Kruger, CR Appledorn and PY Liu. 'Microwave-Induced Photoacoustic Sonography.' *9th International Conference on Photoacoustic and Photothermal Phenomena (ICPPP)*, 1996, S598-S601.
- [20] Robert A. Kruger, Daniel R. Reinecke and Gabe A. Kruger. 'Thermoacoustic computed tomography – technical considerations.' *Med Phys*, 1999, **26**, p.1832-1837.
- [21] Liu Pingyu. 'The P-transform and photoacoustic image reconstruction.' *Phys Med Biol*, 1998, **43**, p.667-674.
- [22] Christoph G. A. Hoelen and Frits F. M. de Mul. 'Image reconstruction for photoacoustic scanning of tissue structures.' *Appl Optics*, 2000, **39**, p.5872-5883.
- [23] C. G. A. Hoelen, F. F. M. de Mul, R. Pongers and A. Dekker. 'Three-dimensional photoacoustic imaging of blood vessels in tissue.' *Opt Lett*, 1998, **23**, p.648-650.
- [24] Kornel P. Köstli, Martin Frenz, Heinz P. Weber, Günther Paltauf and Heinz Schmidt-Kloiber. 'Optoacoustic tomography: time-gated measurement of pressure distributions and image reconstruction.' *Appl Optics*, 2001, **40**, p.3800-3809.
- [25] G. Paltauf, J. A. Viator, S. A. Prahl and S. L. Jacques. 'Iterative reconstruction algorithm for optoacoustic imaging.' *The Journal of the Acoustical Society of America*, 2002, **112**, p.1536-1544.
- [26] Yulia V. Zhulina. 'Optimal statistical approach to optoacoustic image reconstruction.' *Appl Optics*, 2000, **39**, p.5971-5977.
- [27] Robert A. Kruger, Kathy D. Miller, Handel E. Reynolds, William L. Kiser, Daniel R. Reinecke and Gabe A. Kruger. 'Breast Cancer in Vivo: Contrast Enhancement with Thermoacoustic CT at 434 MHz — Feasibility Study.' *Radiology*, 2000, **216**, p.279-283.

- [28] Robert A. Kruger, Keith Stantz and William L. Jr Kiser. 'Thermoacoustic CT of the breast.' *Medical Imaging 2002: Physics of Medical Imaging*, 2002, p.521-525.
- [29] Robert A. Kruger, Kenyon K. Kopecky, Alex M. Aisen, Daniel R. Reinecke, Gabe A. Kruger and William L. Kiser. 'Thermoacoustic CT with Radio Waves: A Medical Imaging Paradigm.' *Radiology*, 1999, **211**, p.275-278.
- [30] Robert A. Kruger, William L. Kiser, Daniel R. Reinecke and Gabe A. Kruger. 'Thermoacoustic computed tomography using a conventional linear transducer array.' *Med Phys*, 2003, **30**, p.856-860.
- [31] Robert A. Kruger, William L. Kiser, Daniel R. Reinecke, Gabe A. Kruger and Kathy D. Miller. 'Thermoacoustic molecular imaging of small animals.' *Molecular imaging*, 2003, **2**, p.113-123.
- [32] A. A. Karabutov, E. V. Savateeva and A. A. Oraevsky. 'Optoacoustic Tomography: New Modality of laser diagnostic systems.' *Laser Phys*, 2003, **13**, p.711-723.
- [33] R. O. Esenaliev, Alexander A. Karabutov and A. A. Oraevsky. 'Sensitivity of laser opto-acoustic imaging in detection of small deeply embedded tumors.' *Ieee J Sel Top Quant*, 1999, **5**, p.981-988.
- [34] Alexander A. Oraevsky, Alexander A. Karabutov, Sergey V. Solomatin, Elena V. Savateeva, Valeri A. Andreev, Zoran Gatalica, Harbans Singh and R. Declan Fleming. 'Laser optoacoustic imaging of breast cancer in vivo.' 2001, p.6-15.
- [35] Louis-S Bouchard, M. Sabieh Anwar, Gang L. Liu, Byron Hann, Z. Harry Xie, Joe W. Gray, Xueding Wang, Alexander Pines and Fanqing Frank Chen. 'Picomolar sensitivity MRI and photoacoustic imaging of cobalt nanoparticles.' *P Natl Acad Sci Usa*, 2009, **106**, p.4085-4089.
- [36] Xueding Wang, Yongjiang Pang, Geng Ku, Xueyi Xie, George Stoica and Lihong V. Wang. 'Noninvasive laser-induced photoacoustic tomography for structural and in vivo functional in vivo imaging of the brain.' *Nat Biotechnol*, 2003, **21**, p.803-806.
- [37] Xueding Wang, Yongjiang Pang, Geng Ku, George Stoica and Lihong V. Wang. 'Three-dimensional laser-induced photoacoustic tomography of mouse brain with the skin and skull intact.' *Opt Lett*, 2003, **28**, p.1739-1741.
- [38] Kornel P. Kostli, D. Frauchiger, J. J. Niederhauser, Gunther Paltauf, H. P. Weber and Martin Frenz. 'Optoacoustic imaging using a three-dimensional reconstruction algorithm.' *Ieee J Sel Top Quant*, 2001, **7**, p.918-923.
- [39] G. Paltauf, H. Schmidt-Kloiber, K. P. Köstli and M. Frenz. 'Optical method for two-dimensional ultrasonic detection.' *Appl Phys Lett*, 1999, **75**, p.1048-1050.
- [40] J. J. Niederhauser, M. Jaeger and M. Frenz. 'Real-time three-dimensional optoacoustic imaging using an acoustic lens system.' *Appl Phys Lett*, 2004, **85**, p.846-848.
- [41] Kharine and Srirang Manohar de Alexei. 'Poly(vinyl alcohol) gels for use as tissue phantoms in photoacoustic mammography.' *Phys Med Biol*, 2003, **48**, p.357-370.

- [42] Xu Minghua and L. V. Wang. 'Time-domain reconstruction for thermoacoustic tomography in a spherical geometry.' *Ieee T Med Imaging*, 2002, **21**, p.814-822.
- [43] Xu Yuan, Xu Minghua and L. V. Wang. 'Exact frequency-domain reconstruction for thermoacoustic tomography. II. Cylindrical geometry.' *Ieee T Med Imaging*, 2002, **21**, p.829-833.
- [44] Xu Yuan, Feng Dazi and L. V. Wang. 'Exact frequency-domain reconstruction for thermoacoustic tomography. I. Planar geometry.' *Ieee T Med Imaging*, 2002, **21**, p.823-828.
- [45] P. Köstli and Martin Kornel. 'Temporal backward projection of optoacoustic pressure transients using Fourier transform methods.' *Phys Med Biol*, 2001, **46**, p.1863-1872.
- [46] Guenther Paltauf, Robert Nuster, Markus Haltmeier and Peter Burgholzer. 'Photoacoustic tomography using a Mach-Zehnder interferometer as an acoustic line detector.' *Appl Optics*, 2007, **46**, p.3352-3358.
- [47] Xueding Wang, David L. Chamberland and David A. Jamadar. 'Noninvasive photoacoustic tomography of human peripheral joints toward diagnosis of inflammatory arthritis.' *Opt Lett*, 2007, **32**, p.3002-3004.
- [48] Daniel Razansky, Claudio Vinegoni and Vasilis Ntziachristos. 'Multispectral photoacoustic imaging of fluorochromes in small animals.' *Opt Lett*, 2007, **32**, p.2891-2893.
- [49] Li Meng-Lin, Oh Jung-Taek, X. Xie, G. Ku, Wang Wei, Li Chun, G. Lungu, G. Stoica and L. V. Wang. 'Simultaneous Molecular and Hypoxia Imaging of Brain Tumors In Vivo Using Spectroscopic Photoacoustic Tomography.' *P Ieee*, 2008, **96**, p.481-489.
- [50] Lao and Da Xing Yeqi. 'Noninvasive photoacoustic imaging of the developing vasculature during early tumor growth.' *Phys Med Biol*, 2008, **53**, p.4203-4212.
- [51] Sergey A. Ermilov, Tuenchit Khamapirad, Andre Conjusteau, Morton H. Leonard, Ron Lacewell, Ketan Mehta, Tom Miller and Alexander A. Oraevsky. 'Laser optoacoustic imaging system for detection of breast cancer.' *J Biomed Opt*, 2009, **14**, p.24007.
- [52] Roger J. Zemp, Liang Song, Rachel Bitton, K. K. Shung and Lihong V. Wang. 'Realtime photoacoustic microscopy in vivo with a 30-MHz ultrasound array transducer.' *Opt Express*, 2008, **16**, p.7915-7928.
- [53] Jung-Taek Oh, Meng-Lin Li, Hao F. Zhang, Konstantin Maslov, George Stoica and Lihong V. Wang. 'Three-dimensional imaging of skin melanoma in vivo by dual-wavelength photoacoustic microscopy.' *J Biomed Opt*, 2006, **11**, p.34032.
- [54] Bin Rao, Li Li, Konstantin Maslov and Lihong Wang. 'Hybrid-scanning optical-resolution photoacoustic microscopy for in vivo vasculature imaging.' *Opt Lett*, 2010, **35**, p.1521-1523.

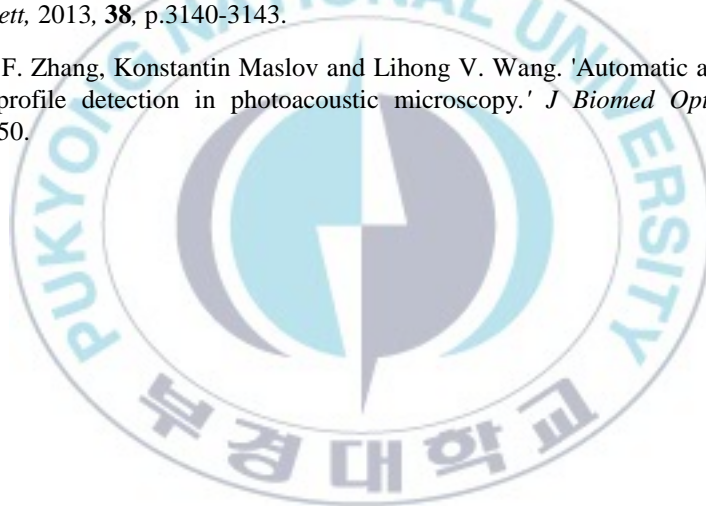
- [55] Song Hu, Konstantin Maslov, Vassiliy Tsytsev and Lihong V. Wang. 'Functional transcranial brain imaging by optical-resolution photoacoustic microscopy.' *J Biomed Opt*, 2009, **14**, p.40503.
- [56] Erich W. Stein, Konstantin Maslov and Lihong V. Wang. 'Noninvasive, in vivo imaging of blood-oxygenation dynamics within the mouse brain using photoacoustic microscopy.' *J Biomed Opt*, 2009, **14**, p.20502.
- [57] Hao F. Zhang, Konstantin Maslov, George Stoica and Lihong V. Wang. 'Imaging acute thermal burns by photoacoustic microscopy.' *J Biomed Opt*, 2006, **11**, p.54033.
- [58] Shuliang Jiao, Zhixing Xie, Hao F. Zhang and Carmen A. Puliafito. 'Simultaneous multimodal imaging with integrated photoacoustic microscopy and optical coherence tomography.' *Opt Lett*, 2009, **34**, p.2961-2963.
- [59] Jan Laufer, Edward Zhang, Gennadij Raivich and Paul Beard. 'Three-dimensional noninvasive imaging of the vasculature in the mouse brain using a high resolution photoacoustic scanner.' *Appl Optics*, 2009, **48**, p.D299-D306.
- [60] Z. Zhang and J. E. 'In vivo high-resolution 3D photoacoustic imaging of superficial vascular anatomy.' *Phys Med Biol*, 2009, **54**, p.1035-1046.
- [61] Edward Zhang, Jan Laufer and Paul Beard. 'Backward-mode multiwavelength photoacoustic scanner using a planar Fabry-Perot polymer film ultrasound sensor for high-resolution three-dimensional imaging of biological tissues.' *Appl Optics*, 2008, **47**, p.561-577.
- [62] L. Chamberland and Ashish David. 'Photoacoustic tomography of joints aided by an Etanercept-conjugated gold nanoparticle contrast agent—an ex vivo preliminary rat study.' *Nanotechnology*, 2008, **19**, p.95101.
- [63] Xueding Wang, David L. Chamberland, Paul L. Carson, J. Brian Fowlkes, Ronald O. Bude, David A. Jamadar and Blake J. Roessler. 'Imaging of joints with laser-based photoacoustic tomography: An animal study.' *Med Phys*, 2006, **33**, p.2691-2697.
- [64] Burgholzer and J. Bauer-Marschallinger P. 'Temporal back-projection algorithms for photoacoustic tomography with integrating line detectors.' *Inverse Probl*, 2007, **23**, p.S65-S80.
- [65] G. Paltauf, R. Nuster and P. Burgholzer. 'Characterization of integrating ultrasound detectors for photoacoustic tomography.' *J Appl Phys*, 2009, **105**, p.102026-102029.
- [66] Jithin Jose, Srirang Manohar, Roy G. M. Kolkman, W. Steenbergen and Ton G. van Leeuwen. 'Imaging of tumor vasculature using Twente photoacoustic systems.' *Journal of Biophotonics*, 2009, **2**, p.701-717.
- [67] R. I. Siphanto, K. K. Thumma, R. G. M. Kolkman, T. G. van Leeuwen, F. F. M. de Mul, J. W. van Neck, L. N. A. van Adrichem and W. Steenbergen. 'Serial noninvasive photoacoustic imaging of neovascularization in tumor angiogenesis.' *Opt Express*, 2005, **13**, p.89-95.

- [68] R. J. Zemp, L. Song, R. Bitton, K. K. Shung and L. V. Wang. 'Realtime Photoacoustic Microscopy of Murine Cardiovascular Dynamics.' *Opt Express*, 2008, **16**, p.18551-18556.
- [69] J. J. Niederhauser, M. Jaeger, R. Lemor, P. Weber and Martin Frenz. 'Combined ultrasound and optoacoustic system for real-time high-contrast vascular imaging in vivo.' *Ieee T Med Imaging*, 2005, **24**, p.436-440.
- [70] John Gamelin, Anastasios Maurudis, Andres Aguirre, Fei Huang, Puyun Guo, Lihong V. Wang and Quing Zhu. 'A real-time photoacoustic tomography system for small animals.' *Opt Express*, 2009, **17**, p.10489-10498.
- [71] Vladimir P. Zharov, Ekaterina I. Galanzha, Evgeny V. Shashkov, Jin-Woo Kim, Nikolai G. Khlebtsov and Valery V. Tuchin. 'Photoacoustic flow cytometry: principle and application for real-time detection of circulating single nanoparticles, pathogens, and contrast dyes in vivo.' *J Biomed Opt*, 2007, **12**, p.51503.
- [72] Liang Song, Konstantin Maslov, Rachel Bitton, K. Kirk Shung and Lihong V. Wang. 'Fast 3-D dark-field reflection-mode photoacoustic microscopy in vivo with a 30-MHz ultrasound linear array.' *J Biomed Opt*, 2008, **13**, p.54028.
- [73] H. W. Edward and T. A. Ford. 'Polyvinylidene fluoride and process for obtaining the same.' 1948.
- [74] Kawai Heiji. 'The Piezoelectricity of Poly (vinylidene Fluoride).' *Jpn J Appl Phys*, 1969, **8**, p.975-976.
- [75] E. Fukada. 'History and recent progress in piezoelectric polymers.' *IEEE transactions on ultrasonics, ferroelectrics, and frequency control*, 2000, **47**, p.1277-1290.
- [76] E. Fukada. 'History and recent progress in piezoelectric polymer research.' 1998, **1**, p.597-605
- [77] L. F. Brown. 'Ferroelectric polymers: current and future ultrasound applications.' 1992, p.539-550
- [78] Lewis F. Brown. 'New developments in piezoelectric polymer ultrasound transducers and transducer systems.' 1992, **1733**, p.27-36
- [79] P. M. Galletti, D. E. De Rossi and A. S. DeReggi. 'Medical Applications of Piezoelectric Polymers.' *Journal of Clinical Engineering*, 1989, **14**, p.84.
- [80] H. Ohigashi, T. T. Wang, J. M. Herbert and A. M. Glass. 'The applications of ferroelectric polymers.' 1989, **40**, p.222
- [81] F. Stuart Foster, Marcel Arditi and John W. Hunt. 'Cylindrical transducer scatter scanner.' *The Journal of the Acoustical Society of America*, 1980, **68**, p.85-92.
- [82] Jong Seob Jeong and K. Kirk Shung. 'Improved fabrication of focused single element P(VDF - TrFE) transducer for high frequency ultrasound applications.' *Ultrasonics*, 2013, **53**, p.455-458.

- [83] J. A. Ketterling, O. Aristizabal, D. H. Turnbull and F. L. Lizzi. 'Design and fabrication of a 40-MHz annular array transducer.' *IEEE transactions on ultrasonics, ferroelectrics, and frequency control*, 2005, **52**, p.672-681.
- [84] O. Arsitizabal, D. H. Turnbull, J. Mamou and J. A. Ketterling. '40 MHz annular-array in utero imaging of mouse embryos with chirp coded excitation.' *2008*, p.126-129
- [85] S. J. Carey, Christian Brox-Nilsen, H. Lewis, C. Gregory and J. V. Hatfield. 'Scanning Head with 128-Element 20-MHz PVDF Linear Array Transducer.' *IEEE transactions on ultrasonics, ferroelectrics, and frequency control*, 2009, **56**, p.1769-1777.
- [86] Sheng-Wen Huang, Sung-Liang Chen, Tao Ling, Adam Maxwell, Matthew O Donnell, L. Jay Guo and Shai Ashkenazi. 'Low-noise wideband ultrasound detection using polymer microring resonators.' *Appl Phys Lett*, 2008, **92**, p.193509.
- [87] Aravind and P. C. M. 'Thermal parameter measurements of bulk YBCO superconductor using PVDF transducer.' *Measurement Science and Technology*, 1999, **10**, p.979-985.
- [88] H. E. Karrer and J. Leach. 'A Quartz Resonator Pressure Transducer.' *IEEE Transactions on Industrial Electronics and Control Instrumentation*, 1969, **IECI-16**, p.44-50.
- [89] Bo Zhang, Qionguo Mao, Xue Zhang, Tianlun Jiang, Ming Chen, Fan Yu and Weiling Fu. 'A novel piezoelectric quartz micro-array immunosensor based on self-assembled monolayer for determination of human chorionic gonadotropin.' *Biosensors and Bioelectronics*, 2004, **19**, p.711-720.
- [90] W. G. Cady. 'The Piezo-Electric Resonator.' *Proceedings of the Institute of Radio Engineers*, 1922, **10**, p.83-114.
- [91] George Washington Pierce. 'Piezoelectric crystal resonators and crystal oscillators applied to the precision calibration of wavemeters.' Published by *American Academy of Arts and Sciences*, 1923.
- [92] S. W. Choi, R. T. R. ShROUT, S. J. Jang and A. S. Bhalla. 'Dielectric and pyroelectric properties in the  $\text{Pb}(\text{Mg}_{1/3}\text{Nb}_{2/3})\text{O}_3\text{-PbTiO}_3$  system.' *Ferroelectrics*, 1989, **100**, p.29-38.
- [93] Chen Jie and R. Panda. 'Review: commercialization of piezoelectric single crystals for medical imaging applications.' *2005*, **1**, p.235-240
- [94] S. Saitoh, T. Takeuchi, T. Kobayashi, K. Harada, S. Shimanuki and Y. Yamashita. 'A 3.7 MHz phased array probe using  $0.91\text{Pb}(\text{Zn}_{1/3}\text{Nb}_{2/3})\text{O}_3\text{-}0.09\text{PbTiO}_3$ .' *IEEE transactions on ultrasonics, ferroelectrics, and frequency control*, 1999, **46**, p.414-421.
- [95] C. G. Oakley and M. J. Zipparo. 'Single crystal piezoelectrics: a revolutionary development for transducers.' *2000*, **2**, p.1157-1167

- [96] T. Ritter, Geng Xuechang, K. K. Shung, P. D. Lopath, Seung-Eek Park and Thomas R. Shrout. 'Single crystal PZN/PT-polymer composites for ultrasound transducer applications.' *IEEE transactions on ultrasonics, ferroelectrics, and frequency control*, 2000, **47**, p.792-800.
- [97] Zhou Qifa, Xu Xiaochen, E. J. Gottlieb, Sun Lei, J. M. Cannata, H. Ameri, M. S. Humayun, Han Pengdi and K. K. Shung. 'PMN-PT single crystal, high-frequency ultrasonic needle transducers for pulsed-wave Doppler application.' *IEEE transactions on ultrasonics, ferroelectrics, and frequency control*, 2007, **54**, p.668-675.
- [98] Joon-Mo Yang, Ruimin Chen, Christopher Favazza, Junjie Yao, Qifa Zhou, K. Kirk Shung and Lihong V. Wang. 'A 2.5-mm outer diameter photoacoustic endoscopic mini-probe based on a highly sensitive PMN-PT ultrasonic transducer.' *2012*, **8223**, p.82233M
- [99] Xiang Li, Wei Wei, Qifa Zhou, K. Kirk Shung and Zhongping Chen. 'Intravascular photoacoustic imaging at 35 and 80 MHz.' *2012*, **17**, p.1060051-1060056.
- [100] Krista Jansen, Min Wu, Antonius F. W. van der Steen and Gijs van Soest. 'Photoacoustic imaging of human coronary atherosclerosis in two spectral bands.' *2014*, **2**, p.12-20.
- [101] B. Jaffe, R. S. Roth and S. Marzullo. 'Piezoelectric Properties of Lead Zirconate - Lead Titanate Solid - Solution Ceramics.' *J Appl Phys*, 1954, **25**, p.809-810.
- [102] Masatsune Yamaguchi, KEN-YA HASHIMOTO, R. Nanjo, N. Hanazawa, S. Ttsutsumi and T. Yonezawa. 'Ultrasonic properties of PZT thin films in UHF-SHF ranges-prepared by sol gel method.' *1997*, p.544-551
- [103] M. Lukacs, Michael Sayer and S. Foster. 'Single element high frequency (<50 MHz) PZT sol gel composite ultrasound transducers.' *IEEE transactions on ultrasonics, ferroelectrics, and frequency control*, 2000, **47**, p.148-159.
- [104] F. Stuart Foster, James Mehi, Marc Lukacs, Desmond Hirson, Chris White, Chris Chaggares and Andrew Needles. 'A New 15 - 50 MHz Array-Based Micro-Ultrasound Scanner for Preclinical Imaging.' *Ultrasound in Medicine & Biology*, 2009, **35**, p.1700-1708.
- [105] R. E. Newnham, D. P. Skinner and L. E. Cross. 'Connectivity and piezoelectric-pyroelectric composites.' *Mater Res Bull*, 1978, **13**, p.525-536.
- [106] R. E. Newnham, L. J. Bowen, K. A. Klicker and L. E. Cross. 'Composite piezoelectric transducers.' *Mater Design*, 1980, **2**, p.93-106.
- [107] Zuomin Zhao and Risto Myllylä. 'The effects of optical scattering on pulsed photoacoustic measurement in weakly absorbing liquids.' *Measurement Science and Technology*, 2001, **12**, p.2172-2177.
- [108] Kwang Hyun Song and Lihong V. Wang. 'Deep reflection-mode photoacoustic imaging of biological tissue.' *2007*, **12**, p.60503.

- [109] Xueding Wang, David L. Chamberland and Guohua Xi. 'Noninvasive reflection mode photoacoustic imaging through infant skull toward imaging of neonatal brains.' 2008, **168**, p.412-421.
- [110] T. A. Ritter, Thomas R. Shrout, R. Tutwiler and K. K. Shung. 'A 30-MHz piezo-composite ultrasound array for medical imaging applications.' 2002, **49**, p.217-230.
- [111] Thomas Chaigne, Jérôme Gateau, Ori Katz, Emmanuel Bossy and Sylvain Gigan. 'Light focusing and two-dimensional imaging through scattering media using the photoacoustic transmission matrix with an ultrasound array.' *Opt Lett*, 2014, **39**, p.2664-2667.
- [112] Lihong V. Wang. 'Multiscale photoacoustic microscopy and computed tomography.' 2009, **3**, p.503-509.
- [113] Jun Xia, Chao Huang, Konstantin Maslov, Mark A. Anastasio and Lihong V. Wang. 'Enhancement of photoacoustic tomography by ultrasonic computed tomography based on optical excitation of elements of a full-ring transducer array.' *Opt Lett*, 2013, **38**, p.3140-3143.
- [114] Hao F. Zhang, Konstantin Maslov and Lihong V. Wang. 'Automatic algorithm for skin profile detection in photoacoustic microscopy.' *J Biomed Opt*, 2009, **14**, p.24050.



## 국문 요약

# 광음향 영상화를 위한 PVDF 와 PMN-PZT 초음파 트랜스듀서 개발

曹永刚 (Cao Yonggang)

국립 부경대학교 대학원 물리학과

## 국문 요약

광음향 영상화(photoacoustic imaging)는 의료진단, 생의학 등의 여러 가지 분야에서 적용될 가능성이 높은 새로운 영상기법 중의 하나이다. 이 영상기술은, 높은 대비(contrast)를 갖는 광영상법과 높은 분해능을 갖는 초음파 영상법이, 서로 결합된 복합기법이다. 그것은 재료나 생체에서의 광음향 효과에 기초하며, 레이저가 발생하는 초음파 신호를 탐지하기 위해서 초음파 트랜스듀서를 사용한다. 광음향 시스템에서는 초음파 트랜스듀서가 가장 중요한 요소 중에 하나이다. 그 초음파 트랜스듀서는 단일 소자, 선 배열 또는 곡면 배열로 만들어진다. 많은 연구자들이 고 분해능의 생체 영상을 얻기 위하여 원형 배열 트랜스듀서를 사용 하고 있다. 그러나 그 트랜스듀서의 수신 감도는, 작은 광음향 신호를 탐지하기 위해서는 아직까지도 충분치 못하다.

본 연구의 목적은 저주파 광음향 영상화에 일반적으로 사용되고 있는 1-10 MHz 주파수 대역에서 높은 수신감도를 갖는 초음파 트랜스듀서를

개발하는데 있다. 여기서는 PVDF 압전막을 사용한 단일 소자 평면 트랜스듀서와 120 개의 압전 요소를 갖는 원형 배열 트랜스듀서를 개발하였다. 또한 PMN-PZT 압전 단결정을 사용하여 극소형 트랜스듀서(needle hydrophone)와 그것을 120 개 배열한 원형 트랜스듀서를 개발하였다. 각 트랜스듀서의 펄스-에코 특성을 측정하여 비교하였으며, 비파괴 검사용의 트랜스듀서를 음원으로 사용하여 제작한 각 트랜스듀서의 수신특성을 비교, 평가하였다.

제작된 단일 소자 트랜스듀서에 대한 특성을 요약하면, PVDF 는 중심주파수가 약 10.1 MHz 이고, -6 dB 대역폭은 9.2 MHz 로서 비대역이 91.1%였다. 한편, PMN-PZT 는 중심주파수가 6.2 MHz 이며, -6 dB 대역폭은 5.6 MHz 로서 비대역이 90.3%로 나타났다. 원형배열 트랜스듀서의 경우, PVDF 는 단일 소자와 달리 CCP 에 압전막을 부착하여 제작하였는데, 중심주파수가 11.3 MHz 이고, 비대역이 50.4%로 나타났다. PMN-PZT 는 단일 소자와 동일하게 제작하였으므로, 특성이 같다. 또한, 비파괴 검사용 트랜스듀서를 음원으로 사용한 수신 감도 특성의 측정 결과로부터 PMN-PZT 트랜스듀서가 PVDF 에 비해 약 1.5 배 정도 큰 수신 전압을 나타내었다.

개발된 각 트랜스듀서를 광음향영상 획득에 적용하였다. 단일 소자 트랜스듀서는 주사형 초음파 현미경과 같이 기계적으로 스캐닝하면서 광음향 신호를 수신하여 영상화하였다. 동일한 표적에 대해 PMN-PZT 가 수신한 광음향 신호는 PVDF 에 비해 약 3 배 크게 나타났다. 따라서 영상의 질 또한 PMN-PZT 에 의한 것이 PVDF 에 의한 것 보다 우수하였다. 원형배열 PMN-PZT 는 토모그래피(tomography) 기법에 기초한 광음향영상 장치에 적용되었다. 그 결과로서 얻어진 영상은 높은

분해능을 가졌는데, 그것은 구동하는 압전 요소의 수와 디스플레이에서의 픽셀의 크기에 의존하였다. 즉, 구동하는 압전 요소의 수가 증가하면 분해능이 증가하였으며, 픽셀의 크기가 증가하면 분해능이 감소하였다. 개발된 PMN-PZT 배열 트랜스듀서의 경우, 압전 요소 수가 60 개 이상이고, 픽셀 크기가 0.5 mm 일 때, 영상의 품질은 가장 우수하였다. 결론적으로, PMN-PZT 압전 단결정은 높은 수신 감도를 가지므로, 배열형으로 제작하여 광음향영상 시스템에 사용할 경우, 분해능이 높은 영상을 얻을 수 있음을 알았다.



# Appendix

## A.1. Concave transducer

Concave transducer is one of the most popular single element transducers which are usually used for PA imaging. The focal zone of this kind of transducer is much smaller than a plane surface transducer with similar aperture. It is very useful for PA imaging which requires high resolution.

Zhang et al.[114] used a transducer with high center frequency (50 MHz) and large numerical aperture (0.44) in their PAM system. They obtained a PA image of subcutaneous microvasculature in a Sprague-Dawley rat with high resolution. Rao et al.[54] reported their hybrid-scanning optical resolution PAM system with a 25 MHz bandwidth concave transducer (focal length 15 mm, material PZT, GE). The axial resolution of the obtained PA images was smaller than 31  $\mu\text{m}$ .

In this study, a PVDF single element concave transducer was fabricated. It was compared with the PVDF single element plane transducer which had been introduced in Section 3.2.1.1.

## A.2. Fabrication of transducer

Figure A.1 shows the structure and photograph of the PVDF single element concave transducer. By comparing with Fig. 3.1, it is found that the concave transducer is very similar to the PVDF plane transducer, except the shape of surface. Actually the fabrication methods of two transducers were almost the same, except the jigs. As shown in Fig A.2, a ball ( $\Phi = 12.5 \text{ mm}$ ) was use to make the concave surface instead of the plane which was shown in Fig. 3.2. And the materials for

making the concave transducer were the same as the ones shown in Table 3.1.

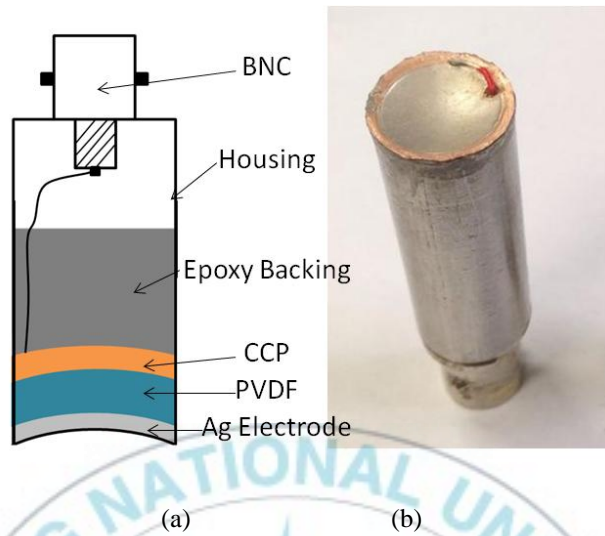


Fig. A.1 Structure (a) and photograph (b) of the PVDF single element concave transducer.

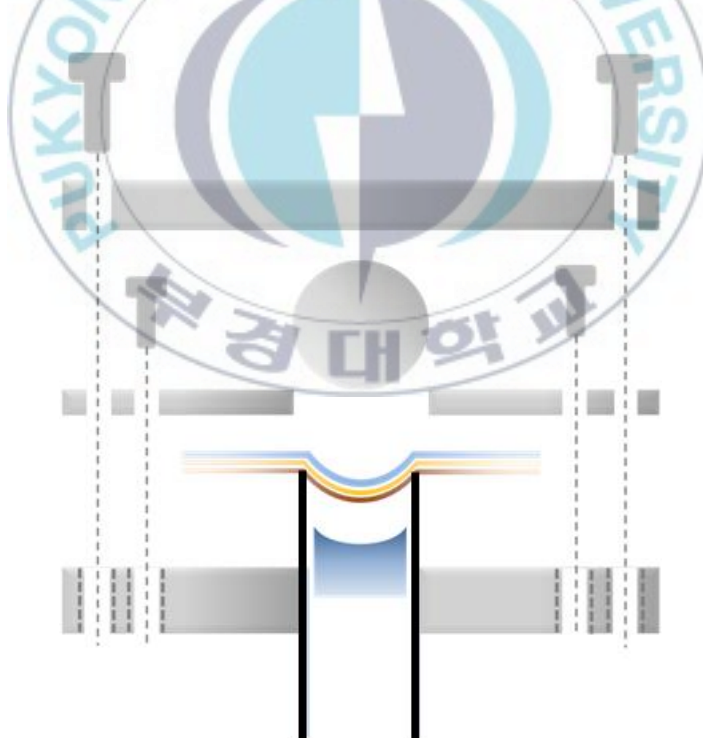


Fig. A.2 Jig for fabrication of the PVDF single element concave transducer

### A.3. Characteristics of transducer

The pulse-echo response and receiving sensitivity of the fabricated PVDF concave transducer were measured and compared with the PVDF plane transducer. The setups for experiments are the same as the ones for the PVDF plane transducer as shown in Fig. 4.1 and Fig. 4.8.

Figure A.3 shows the pulse-echo responses of the PVDF concave transducers. The transducer has the center frequency about 10.2 MHz and -6 dB bandwidth about 9.5 MHz (range: 5.4 ~ 14.9 MHz, 93.1% fractional bandwidth). Both the center frequency and bandwidth are very close to those of the PVDF plane transducer as shown in Fig. 4. 3.

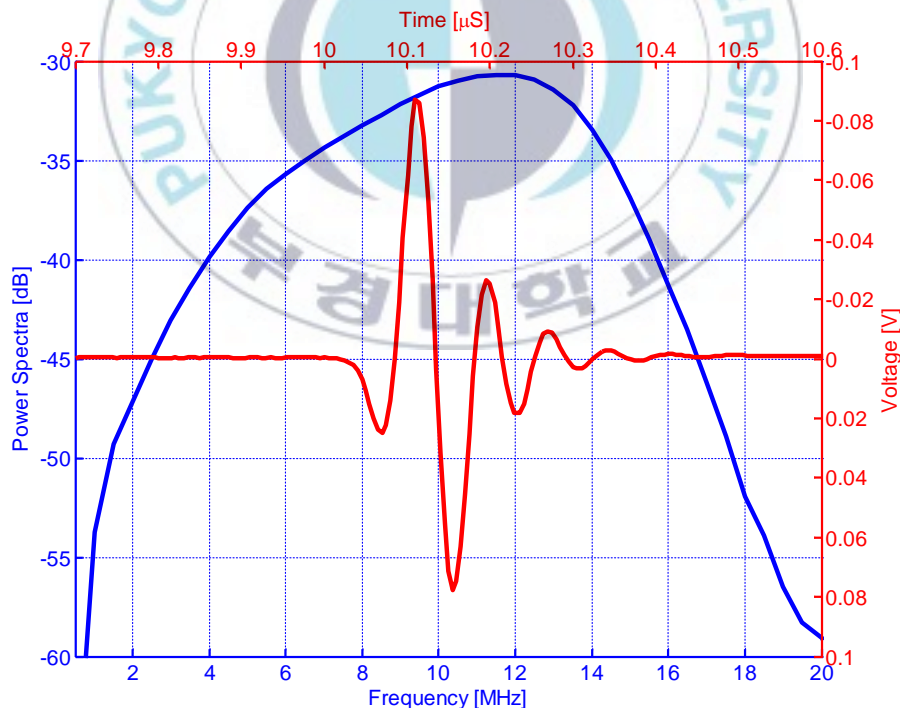


Fig. A.3 Pulse-echo response characteristics of the PVDF concave transducers.

As shown in Fig. A.4, the receiving sensitivity of the PVDF concave transducer is compared with the PVDF plane transducer. The insertion is the reference signal obtained by the commercial PVDF hydrophone. The receiving sensitivity of the concave transducer ( $V_{pp} \approx 150$  mV) is about 3 times higher than the plane transducer ( $V_{pp} \approx 50$  mV).

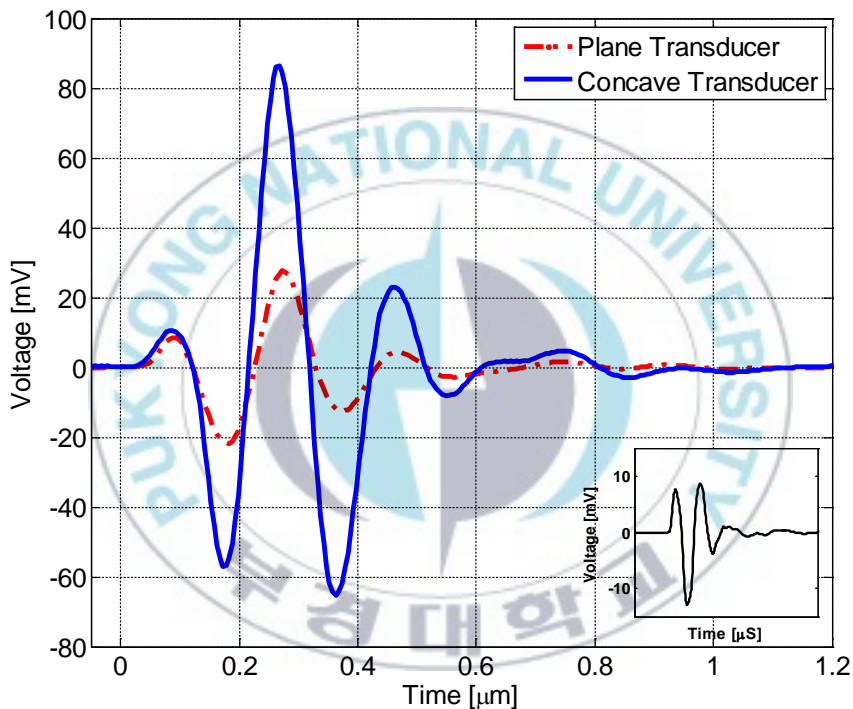


Fig. A.4 Ultrasound signals received by the PVDF concave and plane transducers. (Insertion is the ultrasound signal received by a commercial High Performance PVDF Hydrophone.)

## A.4. PA imaging

The fabricated PVDF concave transducer was applied in a scanning acoustic microscopy approach PA imaging system. The setup and sample for PA imaging were the same as those for PVDF plane transducer, as shown in Fig. 5.2 and 5.4.

Figure A.5 is the PA images by using the concave transducer. It shows that the position of copper wire and bubbles in the sample. By comparing with the PA image by using plane transducer as shown in Fig. 5.5, the concave transducer obtained the PA image with higher quality.

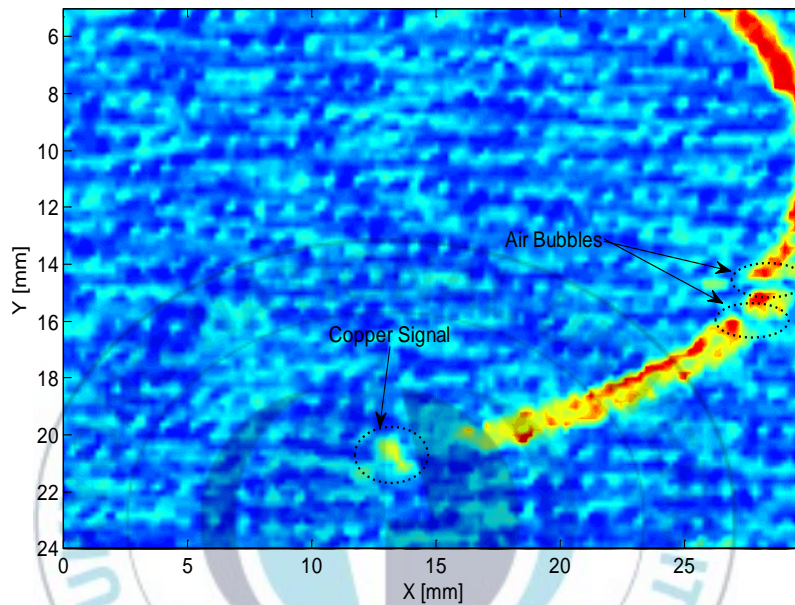


Fig. A.5 PA image obtained by the PVDF concave transducer.

## A.5. Summary

The PVDF single element concave transducer was fabricated. It has similar center frequency and bandwidth as the PVDF plane transducer. However, the concave transducer has 3 times higher receiving sensitivity than the plane one. It can obtain higher quality PA images.

It is useful to use a concave transducer in PA imaging system for high resolution and high contrast image.